Mobile bedform dynamics approaching a bedload parting site:

Armstrong, Christian; Howe, John A.; Allen, Christopher; Watson, Peter

Published in:
Marine Geology
Publication date:
2022

Title: Mobile bedform dynamics approaching a bedload parting site: Pentland Firth, northeast UK

Corresponding author: Christian Armstrong[1]

Christian.Armstrong@sams.ac.uk

John A. Howe[1]

John.Howe@sams.ac.uk

Christopher Allen[1]

Christopher.Allen@srsl.com

Peter Watson[2]

peter.watson@sse.com

Scottish Association for Marine Science, Oban, PA34 1QA [1]

Scottish Hydro Electric Transmission Plc, 10 Henderson Rd, IV1 1SN[2]

Abstract

The Pentland Firth between mainland Scotland and Orkney is an area of the UK continental shelf that experiences extreme tidal flows (>3m/s). This study presents a time series of

bathymetric data coupled with a tidal flow model to examine hydrodynamics and bedform response at the eastern approaches to the Pentland Firth. These observations were additionally augmented by sediment grain type and ADCP data to validate the numerical flow model. Tidal flows of the Pentland Firth result from a tidal phase difference between the east and west approaches to the channel. A resulting barotropic pressure gradient leads to flow accelerations that locally exceed 5m/s. The extreme tidal setting of the Pentland Firth's eastern approach was found to promote distinct bedforms that are spatially varied in geomorphology with distance from the Pentland Firth. Sediment analysis also showed a decreasing grain size trend also with distance from the Pentland Firth. The modelled residual tidal current shows strong agreement with the sediment transport pathways, supported by the bedform migration direction. The energetic tidal flows of the Pentland Firth's eastern approach interacts with the highly irregular coastline, generating residual tidal counter currents leeward of flow obstructions. These counter currents (i.e. residual tidal current vortices) were reflected in bedform migrations and thence the sediment transport pathways. As the Pentland Firth is considered as a bedload parting site, the residual tidal current vortices are expected to influence the rate of erosion at the bedload parting site, by recirculating sediment back upstream as a counter current inshore of the main flow. The modification of sediment transport pathways by residual tidal current vortices may affect the development of nearshore and offshore engineering, and should be considered in any initial site assessment.

1. Introduction

To help mitigate greenhouse gas emission from energy production by fossil fuels, the UK Government has aimed for zero net carbon emissions by 2050 (Pye et al., 2017). As clean

energy alternatives to fossil fuels, significant investment has already been made into harnessing the UK's tide, wind and wave power (Mirzania et al., 2019). The marine renewable energy potential of the UK continental shelf (UKCS) makes nearshore and offshore development particularly appealing. Marine construction requires detailed understanding of the hydrodynamic regime and the ecosystems present, as well as the sediment mechanics for development on and near the seabed (Perkol-Finkel et al., 2018; Sakhaee & Khalili, 2021). The modification of sediment transport pathways is an important consideration for the UK offshore construction sector. However, UK sediment transport pathways before flow modification need to be better understood to appreciate how offshore construction may influence and/or be influenced by the local marine environment in the future.

The UKCS hosts complex sediment transport pathways (Gao & Collins, 1994; Reynaud & Dalrymple, 2012; King et al., 2019). The dominant pathways generally track parallel to the UK's coastline, diverging and converging due to coastal irregularities, island obstructions, and the distribution of tidal amphidromes (Reynaud & Dalrymple, 2012). Where pathways diverge is termed a bedload parting (BLP) site, considered to be the head of the sediment transport stream, with net sediment transport being generally unidirectional away from BLP sites (Harris, 1988). Focussed research into the local sediment mechanics, and the process of sediment transport in hydrodynamic regimes, has been stimulated in part by increasing dependency on coastal engineering interacting with the coastal and nearshore sediment transport regime. However, much less research has focussed on the connectivity of sediment transport pathways between nearshore and offshore environments (Gao et al., 1994; Hooke et al, 1996; Guillou & Chapalain, 2010; Reynaud & Dalrymple, 2012). Considering sediment transport at this larger scale informs on the sediment transport field occurring across the

continental shelf, whilst providing higher resolution insight into nearshore deviations of the sediment transport stream due to coastal inlets and partial flow field obstructions (e.g. islands).

The holistic approach adopted here considering both the local and general sediment transport field has provided a novel perspective of the connectivity between spatiotemporal scales of net sediment transport and the structure of the sediment transport field approaching a BLP: the Pentland Firth, northern UK. By adopting a case study approach to sediment transport, it is possible to assess the seabed's dynamic response to the flow regime, providing some understanding into local seabed mobility. Then examining the case studies in the context of the wider sediment transport field allows insight into the more general seabed stability of the UKCS.

Sediment is transported via three distinct modes: bedload, suspended load, and wash load. Bedload and suspended load transport often produce distinct sediment morphologies termed bedforms. These are accumulations of deposited sediment that are reworked hydraulically (Van Dijk & Lindenbergh, 2017). In the offshore and nearshore submarine environment, bedforms are typically produced in subcritical flow regimes where the Froude number (Fr, quantifying the interaction between inertial and gravitational forces) < 0.84 (Boguchwal & Southard, 1990). A diverse range of bedforms are produced in subcritical flows. This study adopts the classifications of Ashley (1990), where bedforms are broadly distinguished by those whose crest aligns with the dominant flow axis, and those whose crest is oriented obliquely or normal to the dominant flow axis. The ones relevant to this study are banner

93 banks (crest aligned with the dominant flow axis) and dunes (crest aligned obliquely or
94 perpendicularly to the dominant flow axis).

95

96 Banner bank formation is dependent on the hydrodynamics of transient eddy formation
97 (Armstrong et al., 2021; Sigell & Geyer, 1991). In essence, sediment settles out of suspension
98 along the flow shear line (characterised by decreasing horizontal flow speeds) between the
99 main flow and secondary recirculating flow existing in the lee of a flow obstruction (e.g.
100 headland). (Armstrong et al., 2021; Li et al., 2014). Pingree (1978) explained the formation
101 and maintenance of banner banks by residual tidal currents. However, this model has since
102 been deemed inadequate as residual tidal eddies have been identified to not centralise directly
103 above the banner bank crest (Bastos et al., 2003). Alternately, banner banks may be
104 maintained by transient tidal hydrodynamics and non-linear interactions between eddying
105 tidal flows and sediment (Berthot & Pattiaratchi, 2006).

106

107 Dunes on the other hand are wave-like sediment bedforms (Kumbhakar et al., 2017). They
108 range in spacing dependent primarily on the nature of the bed shear stress, sediment supply,
109 and water depth. Their height is limited primarily by the thickness of the bottom flow
110 boundary layer, but also by the grain size (Yalin, 1964; Flemming, 2000). They may be
111 further subcategorised by their geometric scales. *Small dunes* possess wavelengths (defined
112 as crest to crest horizontal spacing) of 0.6-5m and heights (defined as trough to crest vertical
113 length) of 0.075-0.4m. *Medium dunes* possess wavelengths of 5-10m, heights of 0.4-0.75m.
114 *Large dunes* possess wavelengths of 10-100m, heights of 0.75-5m. *Very large dunes* possess
115 wavelengths >100m and heights >5m (Ashley, 1990). Dunes form from an initial bed
116 instability that causes a vertical bottom flow deflection or flow separation (Vittori &

Blondeaux, 1990). Any vertical disturbance in the flow field by the seabed results in local acceleration of the flow and downstream scour of the seabed sediment. The sediment transported from the developing scour site is deposited in a pile downstream, resulting in a second bottom flow instability, perpetuating the process until the flow field dynamics stabilise or the sediment source becomes depleted (Kennedy, 1963; Coleman & Melville, 1996).

A banner bank is considered to be a relatively non-migratory bedform. By contrast, submarine dunes are very mobile, with migration speeds typically being inversely proportional to their volume (Hino, 1968), migrating up to 100m/yr (Van Landeghem et al., 2012), thus representing a significant sediment flux. Dune migration occurs as sediment is transported from the upstream face of the dune, downstream. This leads to erosion of the stoss (upstream) face and deposition on the lee (downstream) face (van den Berg, 1987). In a subcritical bottom flow regime, this typically leads to an asymmetric cross-sectional profile of the dune, characterised by a steep leeward face. In bidirectional (i.e. tidal) flows, dune asymmetry is commonly observed to align with the dominant tidal flow direction also known as the residual tidal current (RTC) as well as the direction of dune migration (Allen, 1980; Fenster et al., 1990).

The residual tidal flow is considered to be the dominant driver of the mean flow field in coastal, near and offshore shelf environments. However, non-astronomic forcing also influences the hydrodynamics. Wind stress on the surface modifies the flow paths and thus alters the mean current (Jones & Davies, 2008). Near the coast, fresh-water introductions by rivers and runoff inhibit the flooding phase of the tide, whilst introducing a volume influx to

141 the local water system, increases the momentum of the ebbing phase (Leonardi et al., 2015).
142 Additional to volume modification, baroclinic gradients by freshwater introduction and
143 thermal heating at the surface stimulate density currents that also alter the mean flow field
144 (Huijts et al., 2009). Significant to offshore development, anthropogenic modification of the
145 physical setting (i.e. coastal, near and offshore construction) locally disrupts the
146 hydrodynamic regime, thus altering the mean flow field and the sediment transport pathways
147 (Haigh et al., 2019).

148

149 Sediment is considered to displace from a BLP site and be transported towards areas of lower
150 hydrodynamic activity where it may become deposited. BLPs indicate where a divergence in
151 the sediment transport field occurs (Harris et al., 1995), typically associated with a similar
152 divergence in the RTC. By contrast, sediment depositions have been associated with
153 converging RTCs, with the pathway from divergence to convergence extending as much as
154 100's of kilometres (Reynaud & Dalrymple, 2012).

155

156 A BLP indicates the head of a sediment transport pathway with bedrock often being exposed
157 due to highly elevated peak current speeds (Belderson & Stride, 1966; Pingree & Griffiths,
158 1979; Van Landeghem et al., 2009). Downstream of the BLP, peak current speed decreases
159 resulting in coarse sediment falling out of suspension. Initial depositional sites are highly
160 reworked hydraulically (Harris & Collins, 1984; Daniell, 2015). Further decreasing
161 hydrodynamic activity downstream also relates to a downstream evolution of bedform
162 morphologies that tend to reduce in size (Belderson et al., 1982).

163

Along with downscaling morphologies, finer sediments fall out of suspension leading to a general downstream decrease in deposited sediment grainsize along the sediment transport pathway (Gao & Collins, 1994). Assessing spatial grain size trends has been somewhat successful inferring sediment transport pathways over large areas of seabed (Cheng et al., 2004; Le Roux & Rojas, 2007; Wang et al., 2020). However, greater affordability of bathymetric data is making repeat multibeam echosounder surveys more achievable. Assessing the spatial distribution of bedforms and their mobility provides an alternative and potentially higher resolution approach to investigating sediment transport pathways on the UKCS.

This study presents results from the analyses of a timeseries bathymetric dataset examining sediment transport pathways proximal to a BLP site. The mobility of bedforms is of direct concern to the offshore construction sector as the lifespan of on offshore installation (e.g. telecommunications cable, wind turbine monopile) may be reduced by seabed instability (Couldrey et al., 2020). Considering the example of a cable or pipeline, seabed instability may lead to free spans where the installed structure is suspended partially in the water column during the self-lowering process. The unaccounted-for stresses may then damage the installation leading to costly maintenance or repair (Leckie et al., 2016). Alternatively, accelerated scour by local flow vortices induced by the flow obstruction may over-deepen the seabed, resulting in exposure of the installation and weakening of the construction's foundations (Hong et al., 2017).

The aims of this seabed assessment are: (1) provide a broad scale analysis of the bathymetric setting at the eastern approach to the Pentland Firth; (2) confirm bedform mobility and

compute bedform migration vectors within newly identified dune fields found in the study area; (3) investigate how the RTC is reflected in the sediment transport field. By completing these aims, we hope to better understand the nature of sediment transport pathways in these highly dynamic and complex seabed settings, aiding future offshore development.

2. Study site

The Pentland Firth (PF) occurs between the northern coast of the Scottish mainland and the southern coast of the Orkney Islands: Hoy, South Walls and South Ronaldsay. Within the PF exists the isles of Stroma and Swona, with the Pentland Skerries presenting a cluster of smaller islands at the PF's eastern approach. The PF ranges between approximately 5-15km wide, and 20km long. Inshore of the isles of Stroma and Swona exist auxiliary flow paths that are ~2.8 and ~4km wide, respectively (figure 1).

The flow paths host flow speeds >5m/s during both the flood (eastward) and ebb (westward) tide (Easton et al., 2012). The highly irregular coastline generates multiple transient eddies and local flow accelerations, resulting in an exceptionally complex flow field. Combined with a mean spring tidal range of 2.8m, the energetic hydrodynamics are due to a tidal phase difference of 2h across the PF, with currents propagating across the channel to equalise the barotropic pressure gradient between the east and west approaches (Adcock et al., 2013).

The strong tidal flows have swept much of the seabed of the PF clean, revealing the underlying Devonian-aged bedrock, composed of mudstone, siltstone and sandstone. The deepest areas of the PF (~100m) exist within the complex network of bedrock faults that are

visible throughout the channel. Sediment deposition does occur within the PF but is restricted to the lee of islands and headlands (British Geological Survey, 2021).

Although bedforms do exist within the PF, this study focusses on its east approach. Here, the principally gravel and sand sediment is transported by a mean flow field that is dominated by the extreme wind, wave and tidal regime of the western North Sea. The sediment transport pathways are further disrupted by flow obstructing headlands and islands, such as the Pentland Skerries. The most distinct sediment deposition of the eastward sediment transport pathway is the Sandy Riddle. Fairley et al. (2015) identified this banner bank as 12km long, with a crestal depth ranging between 16 - 60m beneath the water surface. Superimposed dunes, composed of coarse sand and shell sediment, were reported in abundance along this feature with both wave- and tide-induced currents mobilising sediment across the deposition.

The Sandy Riddle was investigated in Fairley et al. (2015) due in part to the abundance of mobile bedforms present. However, other bedforms have been identified at the PF's eastern approach in high resolution time-series bathymetry data. As far as the authors are aware, these bedforms (excluding the Sandy Riddle) have yet to be reported and have thus been targeted in this study to better understand the wider sediment transport field, downstream of the Pentland Firth.

3. Methods

3.1 Data acquisition and pre processing

3.1.1 Publicly accessible data

A total of 6920km^2 bathymetric data was acquired and analysed from publicly available databases such as UK Hydrographic Office (UKHO), EMODnet, and British Geological Survey (BGS) (figure 1). High resolution depth data was acquired as bathymetric attributed grid format (BAG) from UKHO and reprojected in CARIS HIPS and SIPS v11.1. 29 BAG files were collected with the same vertical datum of mean sea level and assessed by resolution and spatial coverage. The compiled dataset extended from 58.0N - 59.4N latitudinally and -3.8W – -1.3W longitudinally. This represents a coastal area from Tarbet Ness, northeast mainland Scotland, to Tofts Ness, northern Sanday, Orkney isles, and extends offshore for a maximum of 160km. Spatial resolution varied between 2m – 10m, with deeper areas generally possessing lower resolution **(**table 1). The coarser resolution bathymetric map (figures 2 & 10) was downloaded directly from EMODnet, before being georeferenced in QGIS (A Coruña, v.3.10.9), and projected in MATLAB v.2020B .

Sediment and underlying bedrock data were acquired from BGS. Whereas bedrock data was readily mapped, 215 sediment samples were reprocessed and projected in QGIS extending latitudinally and longitudinally from 58.2N – 58.9N and -3.2W – -1.8W, respectively. Sediment was categorised by BGS using Folk & Ward's (1957) classification system. The fractions of gravel (grainsize > 2mm), sand (grainsize = 0.063 – 2mm), and mud (grainsize < 0.063mm) were then extracted for each sample and interpolation of the irregularly spaced datapoints was then performed in MATLAB (figure 3). Interpolation was performed to better visualise the spatial distribution of the three sediment components (gravel, sand and mud) and assess any spatial trends in the data.

Publicly accessible acoustic doppler current profiler (ADCP) data was also downloaded from the British Oceanographic Data Centre (BODC). Numerous datasets were available for the inshore passage between Stroma Island and the northern coast of the Scottish mainland. Intended for model validation (see section 2.3.3), three sampling intervals were selected on

07/04/09: [1] 11:16:45 – 11:45:46, [2] 12:08:10 – 12:26:25, and [3] 12:53:10 – 13:10:56 (all times HH:MM:SS, GMT). All ADCP data were collected during a moving transect using a hull-mounted Teledyne Workhorse Sentinel WHSW-300-I-UG40 ADCP (figure 9). Each transect had a sampling period of 15 seconds containing 12 2m vertical bins, with ~4m range to the first bin, providing horizontal and vertical flow velocities. The depth-averaged horizontal velocities were then computed and geographically projected in MATLAB v.2020B.

3.1.2 Timeseries bathymetric data

Timeseries bathymetric data was collected by MMT Sweden AB using Kongsberg EM710 and EM3002D (both hull-mounted) multibeam echosounder sonars (MBES) covering an area of 74km^2. The initial bathymetric survey was collected between February – March 2013, followed by subsequent survey in 2018. This produced a 78.5km transect of timeseries bathymetry data extending offshore from Noss Head for ~42km before turning 90^o, to continue north, parallel with Orkney's east coast (figures 1, 2, 3 & 8). Whereas the EM710 (frequency range = 40 -100kHz) possesses 256 beams with a swath width up to 140° (data coverage is approximately 5.5 times water depth), the EM3002D operated 160 beams in each of the two sonar heads (frequency range = 293 - 307kHz) with each head possessing a swath width of 130°, producing a typical combined coverage of ~200° (combined data coverage is approximately 10 times water depth). Sound velocity profiles were collected at regular intervals (minimum twice every 24 hours) using a Valeport SVP SVX2. Attitude and inertial positional data were collected using an Applanix POSMV320. Raw data processing was performed in CARIS HIPS & SIPS where depth soundings were georeferenced with tide data (acquired from Global Navigation Satellite System (GNSS) tidal model – cross checked with

local tide gauges) and the total propagated uncertainty (TPU) was computed. The data was then cleaned using combined uncertainty bathymetric evaluation (CUBE) and the bathymetric model projected.

3.2 Data analysis

3.2.1 Bedform morphology assessment

Bedforms were identified in bathymetric data by calculating the surface gradient in QGIS and inspecting areas of non-uniform seabed slope (figure 2). Features were then classified based on their crestal orientation to the coastline as banks (crest oriented parallel to the coast) or dunes (crest oriented obliquely or normal to the coastline). 2D assessment of the features by depth-profile analysis enabled further classification of dunes by scale of morphologic properties (i.e. height, asymmetry and spacing). Height and spacing were predominantly used to distinguish dune by the classification system of Ashley (1990), shown in table 2.

3.2.2 Bedform mobility assessment

Bedform mobility was initially determined by eye assessing spatial evolution of dunes during timeseries bathymetry data. Identified mobile bedforms were then digitised by their crestal position to assess if their mobility was 2- or 3-dimensional. 2D mobility is defined as mass displacement where the structure is preserved during migration. Alternatively, if along-crest net sediment transport is comparable to the transport oriented normal to the bedform crest or if the dune displacement directed normal to the bedform orientation is non-uniform along the crest, dune migration is 3D rendering 2D mobility assessments inadequate. 3D displacement is indicated by bedform deformation during migration presented by analysis of crestal mapping.

3.2.2.1 2D bedform displacement

2D displacement of bedforms were assessed by four estimation methods. Crestal mapping (as above) was used to inspect horizontal displacement of bedform crests. However, this method assumes the accurate digitising of the crests and that the crests remain as a consistent indicator of the centre of mass for the sediment mass transport. For *small* and *medium dunes* that are more susceptible to structural modification by the subordinate tidal flow, the latter assumption is particularly inapplicable. Alternatively, depth profile analysis enabled cross-sectional assessment of the dune features. Asymmetry of *large* and *very large dunes* was used as a useful proxy indicating direction of bedform mobility. However, *small* and *medium dunes* were found to be susceptible to the subordinate tidal flow and thus their asymmetry was deemed inadequate to determine migration direction. On the other hand, depth profiles of timeseries bathymetry across mobile dunes produced a robust method for confirming dune mobility. Moreover, if bedform migration was predominantly 2D, this migration estimation method was found to be an appropriate representation of the displacement along the length of the structure.

3.2.2.2 3D bedform displacement

Two 3D bedform migration estimation methods were applied to timeseries bathymetry data, producing both horizontal and vertical rates of bedform evolution. Using EIVA Helmsman v.4.1 bathymetry software, elevation difference maps were calculated showing the rate of erosion and deposition of sediment within a dune field (figures 6 & 7). Alternating bands of erosion and deposition within a dune field were assumed to indicate dune mobility with depth

shallowing occurring in the direction of displacement as the bedform migrates. This method provided detailed insight into the vertical evolution of individual dunes within a dune field.

Spatial cross correlation was also applied to the timeseries bathymetric dataset. This method has been used frequently on bathymetric data, with notable success from Duffy & Hughes-Clarke (2005) and Buijsman & Ridderinkhof (2008). By considering the dune field as a 3D signal of pixel colour intensities representing the bathymetric gradient, cross correlation estimates the signal's phase shift by double integration of the initial and subsequent spectral field corresponding to the initial and subsequent timeseries bathymetric dataset, respectively (see Duffy & Hughes Clarke (2005) for further details).

Due to the prohibitively extensive scale of the identified bedform fields, a random sampling strategy was adopted, applying cross correlation to randomly selected sites (samples) of dune fields (sample areas). Samples consisted of fields of view (FOV) exported from QGIS. Firstly, the extent of dune fields possessing similarly scaled bedforms were digitised to form sample areas. A random sampling strategy was then implemented by using a random number generator in RStudios to determine the X and Y coordinates of the samples' centroids within the sample area. The number of centroids (and thus samples) scaled proportionally to the total area of a bedform field to account for the decreased relative size of the sample considering an increasing sample area. Samples consisted of 71.6m x 52.1m digitised rectangles that would indicate the FOV to be exported. These dimensions corresponded to a 1:300 scale in QGIS which adequately balanced the FOV's spatial coverage with image resolution. The pixel colour intensities of the exported image were then imported into MATLAB as a matrix representing a 3D signal. The matrix was then gridded into cells. This process was repeated for the subsequent timeseries bathymetric sample, with the subsequent matrix cells scaled to 150% of those from initial sample to capture signal structures that leaked from the initial cell boundary. The grid cells for the subsequent matrix were offset in the direction of

355 displacement (indicated by other methods assessing bedform migration) from the initial
356 matrix aiding the algorithm's signal tracking. Signal displacement was then estimated by
357 spatially cross correlating corresponding cells (initial and subsequent) of the timeseries
358 bathymetric data to produce a vector plot of horizontal displacement.

359 Standard statistical estimators were then calculated for the vector components (u and v) of the
360 vector field. These included: mean, variance, standard deviation, maximum and minimum
361 values. Grid cells were then scaled to find the optimum signal correlation indicated by the
362 lowest variance. The distribution of variance through the dune fields was also found to be a
363 useful estimator of bedform deformation during migration, indicating where the algorithm
364 was less confident in determining the bedform displacement vector due in part to signal
365 decomposition during the signal's phase shift. The mean displacement of the sample's vector
366 field was then projected to form a vector field of mean displacements throughout a sample
367 area (figure 8).
368

369 ### 3.3 DELFT3D

370 DELFT3D-FLOW (tag: 59659) is a numerical modelling system that solves the Navier-
371 Stokes equation by finite difference. The open-source software was configured in sigma-
372 coordinates adopting the Boussinesq assumption of hydrostatic pressure. Further general
373 details of the model may be found in Deltares (2014). An 842 x 302 curvilinear grid was
374 generated with Arakawa-C structure, producing variable spatial resolution throughout the
375 model domain to improve computational efficiency. Resolution ranged from coarse (1.35
376 x1.00km) at the model boundaries (~117km offshore east of Duncansby Head), to fine (90 x
377 120m) at the inshore passage of Stroma.

The model was set up for 2D depth-averaged flow simulation, which was deemed acceptable for the purposes here assuming vertical length scale and velocities are >1 order of magnitude less than that of the horizontal flow. The model was nested within the TPXO Global Inverse Tidal Model (v.8.0) possessing a spatial resolution of 1/12°, with model boundaries being forced by astronomically driven water levels. Tidal modes resolved were semidiurnal (M2, S2, K2, N2) and diurnal (K1, O1, P1, Q1), with baroclinic forcing and riverine outflows omitted for this study. Additionally, wind and wave forcing were also not considered in this model run. A Chezy roughness value of 45 was used for bottom friction that produced a solution of best fit with the ADCP data during model tuning. Due to the resolution of the spatial discretisation, wall effects were expected to be contained within one grid cell of the model coastlines. Thus, model outputs were insensitive to the free slip condition adopted for the coastal boundaries.

The model was run over 14 days: 06/04/2007 (00:00:00 GMT) – 21/04/2007 (00:00:00 GMT) with the initial 24 hours acting as spin-up time allowing the numerical solutions to stabilise. A model time step of 6 seconds ensured the Courant-Friedrichs-Lewy condition was satisfied indicated by a Courant number < 1 (Courant et al., 1928). The RTC flow field was calculated by Fourier analysis of the u and v velocity components and model outputs were visualised and analysed in MATLAB.

To validate the flow model using a moving ADCP track the modelled depth-averaged flow field was time-averaged over the short ADCP sampling interval. Assuming the flow field did not evolve significantly during the ADCP transect, comparing time- and depth-averaged model outputs with the non-stationary ADCP data was deemed a sufficient model validation for the scope of the study. During the three sample intervals, the ADCP recorded a depth-averaged flow vector, oriented westward. The time- and depth-averaged flow model during the same time and space interval measured a comparable decrease in flow speed propagating

403 westward (figure 9). The flow simulation corresponding to Model-1 showed the least
404 agreement between simulation and ADCP data (RMSE = 0.43; R^2 = 0.16). Located the
405 furthest inshore of the three ADCP transects, the maximum flow speed difference was
406 0.85m/s. By comparison, model – 2 (RMSE = 0.18 ; R^2 = 0.79) showed a maximum
407 difference of 0.43m/s, and model – 3 (RMSE = 0.27; R^2 = 0.83) showed a maximum
408 difference 0.2m/s between flow speed and ADCP data. Simulated and real flow speeds were
409 found to consistently diverge at either the beginning or end of the model run, perhaps relating
410 to the short time-averaged approach to the numerical model of an evolving flow system.

411

412

413 ## 4. Results

414 ### 4.1 Study area

415 The seabed depth of the dataset ranged from 5-120m, exhibiting predominantly sediment
416 covered seafloor with the exception of the PF, which presents exposed bedrock. East of the
417 exposed bedrock found within the PF, the sediment has been hydraulically reworked into
418 bedforms classed as *banner banks*, *medium dunes*, *large dunes*, and *very large dunes*.

419 The sediment grabs acquired from BGS indicated a largely mixed sediment composition that
420 is dominated by sand (grainsize = 0.063-2mm, Folk classification). The composition included
421 increasing gravel (grainsize > 2mm) fractions west of the study domain, approaching the PF,
422 and locally at the banner bank extending southeast from the Pentland Skerries, also known as
423 the Sandy Riddle. Towards the east of the study domain, greater fractions of mud (grainsize <
424 0.063) were identified in the sediment composition.

425

4.2 Bedforms

Within the study area, various bedform morphologies were identified as being the likely product of the tidal flows (figure 2). Following the definitions of Ashley (1990) (see table 2) *banner banks, dunes, large dunes,* and *very large dunes* were all observed (figure 4). The dune features are described by broad geographical area in more detail below.

4.2.1 Southeast Approach

The largest of the wave-like bedforms classed as *very large dunes* were found southeast of the PF, north of Noss Head (figure 6). Their wavelengths ranged from 100-150m, with a height of 5-10m. These bedforms possessed strongly asymmetric profiles. However, the southernmost dunes offshore of Noss Head exhibited crests aligned east to west predominantly, with a steep southern face gradient. By contrast, the northernmost dunes approaching the Pentland Firth exhibited crests aligned in a west southwest to east northeast orientation, with a steeper northern face gradient. Individual dune morphologies in southern dunes were relatively self-similar, with crestal bifurcations at the eastern terminals. On the other hand, northern dunes appeared anchored to longer bedforms, oriented northwest to southeast, with induvial dunes again appearing self-similar. Some dunes within this dune field exhibited barchan-like properties with arcuate crests. Very little crestal sinuosity was displayed with the dunes clearly distinguishable and separate from neighbouring bedforms.

4.2.2 East Approach

East of the Pentland Firth, more wave-like bedforms exist proximal to the Pentland Skerries, located centrally within the eastern approaches to the Pentland Firth (Figure 5). Classed as *large* and *very large* dunes (table 2), the bedforms may be distinguished by location, orientation and scale. The largest dunes in this region were located in the eastward lee of the

Pentland Skerries indicated by depth profile 9-10 (figure 5C). These bedforms possessed a height between 6-8m, and a wavelength of 80-120m identifying them as *large* to *very large dunes*. These bedforms were strongly and consistently asymmetric with a steeper west face gradient. Another dune field was located north of these bedforms, that was approximately fan-shaped consisting of dunes with crests aligned predominantly north-south. In the western region of this dune field (nearest the PF), a series of ~200m wide depressions exist leeward of dune crests; the deepest of which is 91m, approximately 25m deeper than the surrounding bathymetric depth. With the exception of these scour pits, dunes of this field were 80-100m wavelength, with a height ranging from 3-6m, defining them as *large dunes*. These dunes possessed less pronounced asymmetry than the *very large dunes* leeward of the Pentland Skerries. However, eastern dune faces were consistently steeper than their western faces.

4.2.3 East Orkney

The seabed east of mainland Orkney and northeast of the Pentland Firth has been reworked into a dune field that extends parallel with the east coast of the Orkney isles (figure 7). These *medium dunes* ranged from 0.6-1m in height with a wavelength of 15-25m typically. The dunes were weakly and inconsistently asymmetric across the field but indicated a large area of sediment transport occurring 25km offshore from Orkney's mainland east coast.

4.2.4 Banner banks

The two most distinguishable banner banks within the study area were those proximal to the PF. Fairley et al. (2015) described the sediment banner bank known as the 'Sandy Riddle'. Approximately 60m (maximum) in height, and 13km long, this deposition is one of the most notable bedform morphologies in the area, and dominates the bathymetric setting. However,

the lack of high-resolution bathymetry data for the feature prevented further analysis of the Sandy Riddle's morphology. The coarse bathymetry data that was publicly available indicated that this banner bank is attached to the Pentland Skerries and extends southeast for approximately 13km, presumably in the lee of the eastward flowing flood tidal stream.

Relatively high-resolution bathymetric data was available for the arcuate banner bank extending 3.5km from the southeast tip of South Ronaldsay (figure 5). Initiating 8km north of the 'Sandy Riddle', this banner bank projects east for 4km before curving south for the remainder of its 11km, for a total 15km length. The maximum height of this feature is approximately 30m, and its cross-sectional asymmetry ranges from symmetrical in the southern section of the bedform, to strongly asymmetric in its central and northern section. The central section of this feature presents a steeper east face gradient, whereas the northern section exhibits a steeper face gradient to the south. Superimposed bedforms were identified on the north and south sections of this banner bank (figure 5A & B).

Banner banks were also identified proximal to Scapa Flow and Stronsay Firth, Orkney isles. However, these were deemed beyond the focus of this paper investigating sediment transport dynamics at the Pentland Firth's east approach.

4.3 Bedform dynamics

Figure 8 shows the results of the cross-correlation analysis of the bathymetric timeseries data, and highlights the migration direction of the sediment and bedform features. The *very large dunes* described in 4.2.1 (figure 6A) were found to migrate in the direction consistent with their asymmetry. The cross-correlation algorithm captured dunes migrating west northwest at the northern extent of the timeseries bathymetry data. These dunes were computed to have migration rate of ~1.5m/yr. By comparison, dunes in the southern section of the field, with

predominantly east-west crestal alignment, were recorded to migrate south with strong agreement between the three estimation methods regarding migration direction. Depth profile analysis showed migration rates ranged between 3-5m/yr; crestal mapping indicated migration rates 2-4m/yr; and the cross-correlation produced the most conserved migration rate estimates of 1.5-2.5m/yr. The area's seabed elevation change was also consistent with a southerly migration direction to the south of figure 6A with erosion of <1.9m on the northern face of the bedforms and accumulation of <0.4m on their southern face.

The timeseries bathymetry transect crossed the east approach of the PF. Along with the bedforms described in 4.2.1, several other sites of bedform mobility were identified where bedform displacement was estimated using the cross-correlation algorithm. Figure 8B shows the migration vectors of a bedform field 23km southeast of the PF. The estimated bedform displacement ranged from 1.5-2.5m/yr in a consistent southeast direction. Figure 8C is located 45km east of the dune field north of Noss Head, and identifies a bedform field with migration vectors that were initially projecting southwest to the south, before the vectors switched to westward projection to the north of domain 8C.

The bedforms of 8D were classed in 4.2.3 as *medium dunes*, with weak and inconsistent asymmetry. The three migration estimation methods were implemented revealing displacement of bedforms during the four-year survey interlude. The estimated bedform migration rate was: 0.7-2m/yr from depth profile analysis and 0.6-0.7m/yr from cross correlation. Crestal analysis produced the most spatially varying migration rates of 0.3-3m/yr. Elevation analysis indicated an eroding north face of the bedforms by <0.08m/yr and an accumulating southern face of <0.05m/yr. This was in strong agreement with the other estimation methods suggesting the bedform migration and thus sediment transport direction was south southeast.

4.4 Hydrodynamic model

4.4.1 Flow model

A maximum difference in sea surface height of 2.1m was found to produce the energetic tidal currents in the PF. Both ebb and flood tides showed current intensification within the constrained channels of the PF and accessory channels. A maximum flow speed of 4.9m/s was recorded during the flood tide to the east north of Stroma's coast (figure 10).

4.4.1.1 Flood stream

Entering the PF from the west, the flood currents began accelerating offshore of Hoy's south coast where the channel begins to constrict the flow (figure 10C). Flow speeds then decreased moving east through the PF until the isles of Stroma and Swona. Here, flow was naturally redirected around the islands' coastlines and into the constrained passageways, reducing the cross-sectional area of the PF, resulting in the greatest current speeds recorded during the flood tide. Flow speeds within the channels between UK mainland, Stroma, Swona, and south Ronaldsay increased to >3m/s with a maximum flow speed recorded of 4.9m/s eastward, north of Stroma's northern shore. Eastward of the flow constriction, currents converged momentarily before being obstructed by the Pentland Skerries, again resulting in increasing flow speeds to the north and south of the easternmost islands. Currents flowing south of the Skerries continued to follow the northeast coast of mainland UK. By contrast currents flowing to the north of the Pentland Skerries presented anticlockwise circulatory dynamics at the flow's northern flanks, and clockwise circulatory dynamics at the southern flank of the eastward tidal projection. Away from the Pentland Firth's eastern

approach, the general flood flow direction was predominantly southward with local current accelerations reflecting protruding coastal headlands and irregularities.

4.4.1.2 Ebb stream

From the east, currents were accelerated across the eastern approach through the passageways bounded by South Ronaldsay, the Pentland Skerries, and the northeast tip of the UK mainland (figure 10D). A leeward eddy formed west of the Pentland Skerries indicated by reversed flow vectors relative to the westward stream. Flow paths converge as the currents enter the PF before separating into three streams. (1) The southernmost stream flowed south around the isle of Stroma before being accelerated within the constricting passageway between Stroma's southern coast and UK mainland's northern coast. This inshore current formed a distinct eddy zone leeward of Stroma, producing a clockwise rotating vortex before re-joining the main flow stream in the centre of the PF flowing west. (2) Between the isles of Stroma and Swona flowed the main current of the PF propagating west northwest with a maximum flow speed of 3.9m/s north of Stroma's northern shore. Current speeds became elevated at the initial constriction between the two islands but remained elevated throughout the transit through the PF, only decelerating after the southwest tip of Hoy. Initially projected to flow west northwest, this central current flowed linearly until redirection by the southern coast of Hoy into a westerly direction. (3) The third stream to the north converged with the mainstream flow (2). This third stream, flowing to the north of Swona island, was projected to flow northwest towards Scapa Flow producing a large eddy to the west of Swona. Before entering Scapa Flow, this current was largely redirected to the southwest due to the obstructions of the isles of Switha and Flotta. This southward current then accelerated along the southeast coast

of South Walls, before converging with the main ebb current propagating centrally through the PF.

4.4.1.3 Residual tidal currents (RTC)

Due to the intricate coastal geometry and interspersed islands of the PF and its approaches, the RTC vector field presented a complex net flow pathway, dominated by flow recirculating eddies (figure 10B). Beginning centrally between the isles of Stroma and Swona, the westward RTC was found to propagate relatively linearly. However, north and south of this central stream occur opposite flowing currents suggesting the eddy zone induced by the presence of the islands strongly influence the RTC pathways away from the central channel. Westward of the isles of Stroma and Swona, the central RTC also recirculated anticlockwise following into the eddy, westward of Stroma Island. RTC magnitudes were mostly elevated near coastlines where the flow was also most constricted (e.g. offshore of Stroma's north coast, and South Ronaldsay's south coast) with the exception of the southeast propagating RTC, dominated by the flood tidal jet.

East of the PF, RTC eddies are very apparent. Inshore of the southeast flowing flood jet the RTC circulated clockwise producing a northward return current towards the PF that accelerated approaching the northeast tip of mainland UK. To the east of the southeast flowing flood jet the RTC recirculated anticlockwise back towards the Pentland Skerries, again accelerating as it reached the head of the eddy. A RTC projecting north of the Pentland Skerries also recirculated clockwise to produce a return current to the PF, again accelerating towards the top of the RTC eddy at the southern tip of South Ronaldsay.

Away from the PF, the general RTC was predominantly southward with local deviations caused by coastal irregularities and headlands. Following the UK mainland coast southward

to Noss Head, the RTC split into a southeast directed current propagating offshore of Noss Head, and a northward return current, tracking back into the PF.

5. Discussion

The energetic tidal flows of the PF are predominantly due to gradients in the tidal barotropic pressure field across the channel. These gradients are dominated by a slope in sea surface height that develops when tidal flows are constrained through the narrow passage between the north coast of mainland UK and south coast of Orkney islands. Flows are further obstructed by several small islands e.g. the Pentland Skerries, Stroma, and Swona. These flow obstructions produce locally accelerated currents, large eddy zones, and combine to form a very flow complex area. The RTC field reflects this complexity exhibiting local accelerations, eddies, and recirculation. Such features of the RTC field are also reflected by intricate and spatially varying net sediment transport pathways identified within the study area.

5.1 Bedform migrations and RTCs

Hydraulically reworked sediment in subcritical flow regimes ($Fr<0.86$) may be characterised by distinct bedform morphologies that reflect the nature of hydrodynamic regime (Boguchwal & Southard, 1990). Bedforms whose crests align with the RTC (e.g. banner banks) are generally characteristic of higher bed shear stresses. Decreasing bed shear stresses typically produces bedforms that are oriented obliquely or perpendicularly to the RTC (e.g. dunes) (Belderson et al., 1982). Observations of bedforms within the PF dataset can thus be indicative of bed shear stress and used as proxies for net sediment transport direction.

5.1.1 Dune mobility

A wide range of dune geometric dimensions were identified in this dataset. It is well reported that dune dimensions scale with the bed shear stress and grain size (Yalin, 1964; Flemming, 2000). The grain size reported here showed a largely mixed sediment composition. This consisted predominantly of sand (0.063 – 2mm) with increasing gravel fraction (>2mm) approaching the PF and at the Sandy Riddle banner bank, contrasted by increasing mud fractions (<0.063) away from the PF to the east in deeper settings. It is suspected that local variations of grain size exist within dune fields. However, spatial resolution of sediment grab samples prevented further investigation.

On the other hand, it is apparent that the bed shear stresses are highly variable spatiotemporally within the study area. Within the PF where bed shear stresses are greatest, bedrock is swept clean of sediment. However, downstream of the PF, where bed shear stresses decrease, sediment has settled out of suspension. Bed shear stresses are still great enough to initiate sediment incipient motion though, resulting in sediment being reworked into bedforms (Allen, 1980; Belderson et al., 1982; Boguchwal & Stride, 1990). The distribution of dunes in particular broadly agreed with the sediment grainsize trends and modelled peak current speed further indicating the variable bed shear stress (Yalin, 1964).

Net sediment transport was also variable at the dune fields in the PF dataset. At the dune field north of Noss Head, bedforms were oriented to a north westerly net sediment transport pathway in the north, and those in the south aligned to a southerly net sediment transport pathway. Furthermore, timeseries bathymetric analysis revealed bedform mobility in agreement with the dunes' asymmetry, with displacement rates ranging from 1.5-5m/yr. This suggests that although bedforms were transported in the direction of the main flood tidal

stream in the south of the dune field, the northern dunes are transported in the opposite direction, back towards the PF. The modelled RTC southeast of the PF indicated a northward residual counter current flowing opposite to the main southward residual current extending from the PF further offshore. This counter current occurred north of Noss Head in agreement with the bedform migrations detected in the Noss Head dune field. South of the northward counter current, approaching Noss Head, the RTC realigns with the main southward RTC projecting from the PF, as do the dune migration vectors. As the RTC predominantly determines the sediment transport pathway, it suspected that the eddying RTC field, induced by coastline irregularities, also transport sediment in the southeast stream from the PF in a recirculating pathway (Cruz & Noernberg, 2020).

Further evidence of recirculating sediment transport was found east of the PF. Bedforms within the fan-shaped dune field to the east of the Pentland Skerries were found to be strongly and consistently asymmetric. The outputs of the modelled RTC strongly suggested that sediment is transported eastward in the channel between South Ronaldsay and the Pentland Skerries. On the other hand, the *very large dune* field identified south of the *large dune* field were also strongly and consistently asymmetric, aligning to a westward current, in the eastern lee of the Pentland Skerries. Oppositely oriented, adjacent sediment transport vectors are consistent with the Noss Head dune field at the southern flank of the PF's eastern approach. This may again be explained by energetic flows propagating past irregular coastline geometries, producing a residual counter current in the eddy zone proximal to the main eastward RTC. The modelled RTC also identified westward counter currents existing in the eastward lee of the Pentland Skerries providing further evidence of this complex sediment transport vector field (Kubicki et al., 2017).

The dunes eastward of the Orkney Isles (Figure 8D) possessed smaller geometric scales than those found closer to the PF. Although weakly and inconsistently asymmetric, the size of the

dune field indicated a significant volume of sediment being transported, motivating further investigation. Timeseries bathymetric analysis revealed a consistently south to south-southwest transport vector across the dune field. The dunes' relatively small morphology may explain their weak and inconsistent asymmetry as being susceptible to the subordinate tidal flow oriented oppositely to the RTC. The modelled RTC further suggested a relatively weak southward RTC in this area, compared to the strong RTCs associated with the PF.

5.1.2 Banner banks

Banner banks in the PF were found adjacent to passageways (e.g. between islands). They are typically associated with coastline irregularities such as headlands and found leeward of flow constrictions where tidal currents were redirected around and accelerated downstream of flow obstructions like the Pentland Skerries. Banner banks are useful proxies for the net sediment transport as they align with the dominant tidal flow axis and indicate that an eddy current may be present, characteristic of energetic tidal flows (Shaw et al., 2012; Li et al., 2014; Traoré et al., 2021).

The banner banks of the eastern approaches to the PF extend south east (Sandy Riddle) and east curving south (Arcuate Bank) (Figure 1). This suggests that the tidal flows are energetically projected south east and east from the Pentland Firth during the flood tide. As such, sediment is therefore transported with the flows and deposited at areas of decreasing flow speeds (i.e. towards eddy zones) forming banner banks.

This agrees with Traoré et al. (2021) that banner banks are maintained by eddies in energetic flows leeward of a flow obstruction. In a simplified conceptual model, the horizontal velocity profile crossing the eddy line is characterised by a zero crossing where the main stream's flow field converges with the eddy counter current's flow field. The reduced flow velocities

approaching the zero crossing results in decreased turbulent suspension force and increased settling velocities, allowing sediment to settle along the eddy line (Armstrong et al., 2021).

This mechanism requires the volumetric flow rate to be significant enough to produce a hydrodynamically stable eddy flow field. In this region a depositional zone can occur where sediment can accumulate and not be hydraulically reworked by flow instabilities developing from the shear between the two opposing currents. Therefore, the formation of leeward depositions (e.g. banner banks) may be dependent on the spatial scale of the flow field. Below a threshold spatial scale, the hydrodynamic instabilities in the flow field may dominate the eddy line preventing sediment accumulation. This may help explain why significant leeward depositions (banner banks) are not as ubiquitous in the marine environment as other bedforms (e.g. dunes).

It is not uncommon to have bedforms such as dunes superimposed on a banner bank (Shaw et al., 2012; Li et al., 2014; Schmitt & Mitchell, 2014; Traoré et al., 2021). Superimposed morphologies are typically mobile, migrating towards the bank's crest in an oblique circulatory pathway relative to the mainstream and counter current. Sediment may then be removed from the top of the bank by episodic surface wave action induced by storm events, eroding the banner bank's crest (Schmitt & Mitchell, 2014).

Although the Sandy Riddle lacked high resolution bathymetry data for further analysis, investigation of the Arcuate Bank to the north was possible. The depth profile analysis indicated the bank's cross-sectional asymmetry varied along its length. This may indicate that the banner bank is subject to secondary net transport across the crest of the feature, shaping the bank similar to a dune. The feature's variable asymmetry agrees with the recirculating RTC that projects eastward through the flow channel between the Pentland Skerries and South Ronaldsay, before circulating anticlockwise back to the PF. Oriented perpendicular to

712 the eastward RTC, the central section of the banner bank possesses a steep east face. By
713 contrast, the northern section is characterised by a steep southern face aligned
714 perpendicularly to the south westward recirculating RTC. This northern component of the
715 banner bank also hosts superimposed dunes that are aligned similar to the crest. It may be that
716 although the dominant flow regime is sufficiently energetic to produce a banner bank, the
717 flow vector field evolves over the tidal cycle to produce currents that become aligned
718 obliquely and even perpendicularly to the banner bank's crest. This would explain the bank's
719 variable asymmetry along its crest in the context of the intricate local RTC pathways.

720 Banner banks in this dataset were observed to be offset from the modelled RTC eddy line.
721 Bastos et al. (2003) also observed a displacement of the banner bank's location from the RTC
722 eddy line, suggesting Pingree's (1978) model must be incomplete when describing the
723 dependency of the banner bank formation on the RTC flow field. Sediment transport is driven
724 by the mean flow field, with tidal currents being dominant on the UKCS. However, other
725 episodic mechanisms may modify the flow field that may not be accounted for in
726 hydrodynamic simulations and thus not considered in the modelled mean flow field (for
727 example: wind stress (Jones & Davies, 2008), and internal tides (Masanuga et al., 2020)).
728 Additionally, further discrepancies may be due to the 2D depth-averaged approach not
729 resolving local bottom hydrodynamics. Berthot & Pattiaratchi (2006) observed complex
730 bottom flows across the banner banks that did not align with the surface flows by LRTC
731 assessment. A vertically non-uniform velocity field may also partly explain the divergence
732 between a modelled depth-averaged RTC and the banner banks' locations.

733

734 ### 5.2 Sediment transport pathways and RTCs

735 The PF is classed as a complete BLP site where seabed areas totally devoid of sediment span
736 the entire width of the flow channel and sediment deposition on either side of the parting site
737 are entirely disconnected (Harris, 1988; Harris & Collins, 1991). The PF thus may be
738 described as the head of a sediment transport pathway that tracks away from the area to the
739 east and west.

740 This study documents a region of the UKCS where sediment transport pathways possess
741 significant deviations from an otherwise generally unidirectional sediment transport stream
742 (Kubicki et al., 2017; Cruz & Noernberg, 2020). This is particularly applicable near a BLP
743 like the PF, characterised by elevated flow speeds and local tidal jet currents in extreme
744 cases. The elevated flow speeds and tidal jets are often accompanied by flow separations
745 around protruding headlands and flow obstructing islands. In the lee of these flow
746 separations, the flow speeds are significantly reduced, and currents are often reversed,
747 producing counter currents that recirculate water back towards the flow deflecting feature.

748 In the case of the PF's eastern approach, eddying tidal flow mechanics are reflected also in
749 the RTC flow field (figure 11). In the flow constricting channels (e.g. between Pentland
750 Skerries and South Ronaldsay), the tidal currents are accelerated. The local current speeds are
751 typically unequal between the flood and ebb tide and this imbalance also varies spatially
752 resulting in complex RTC pathways characterised by a meandering and often recirculating
753 flow field leeward of a flow separating obstruction (e.g. an island).

754 The bedforms observed in this study serve as useful proxies for identifying the mechanisms
755 and pathways of sediment transport. Analysis of the bedform features suggested that the
756 sediment transport pathways largely follow the complex RTC flow field. At the eastern
757 approach to the PF, sediment may be recirculated back towards the BLP. Significant
758 redirection and even reversal of the sediment transport pathway may then occur proximal to a

BLP; particularly towards the flanks of the main flow channel. The recirculation of sediment may be a mechanism that limits the formation of a BLP by recycling sediment towards the area of uncovered seabed bedrock, as opposed to the net sediment transport field being unidirectional.

This sediment transport mechanism should be considered when installing engineered structures offshore, especially when proximal to elevated tidal flows constrained by irregular coastlines. By the insights provided by this dataset, local disruption of the sediment transport stream may result in an upstream starvation of the sediment source if the recirculatory sediment pathways are significantly modified. With less sediment recirculated, the foundational stability of the offshore construction may be risked by scour, elevated by the decreased upstream supply of sediment. This may be particularly relevant to sensitive sediment pathways found in constrained flow areas where sediment supply is already scarce and downstream effects may be more pronounced (Thiébot et al., 2015).

6 Conclusion

The PF is an energetic tidal channel with a tidal phase difference between the east and west approaches promoting a barotropic pressure gradient and thence flow acceleration. Exposed bedrock within the PF indicated that the seabed is swept clean of sediment defining the channel as a BLP. Sediment was found to be deposited downstream of the PF at the eastern approach, with sediment grain sizes showing a slight a decrease from gravelly sand to muddy sand with increasing distance from the PF.

Bedforms were identified downstream of the PF where coarse sediment has fallen out of suspension and subsequently reworked hydraulically by the energetic tidal flows. Two banner banks were identified extending leeward from the Pentland Skerries (‘Sandy Riddle’) and

783 South Ronaldsay (‘Arcuate Bank’). These morphologies are documented to form at the eddy
784 line of two oppositely flowing currents, attached to an erosion resistant feature (e.g. coastal
785 headland). Detailed investigation of the Arcuate Bank was afforded by high resolution
786 bathymetry data with the 15km long banner bank being found to exhibit an asymmetric cross-
787 section that varied along its length. Comparison with the modelled residual tidal current
788 (RTC) showed that the temporal evolution of the tidal flows results in relatively weak flows
789 oriented perpendicularly to the bank’s crest at certain stages of the tidal cycle. The
790 asymmetry of the bank was found to reflect this being asymmetric to the secondary flow axis
791 whilst being structurally maintained by the dominant eastward flood flows extending from
792 the PF.

793 Numerous dune fields were identified within the PF. The largest dune morphologies were
794 identified close to the PF with geometries generally decreasing with decreasing peak flow
795 speeds. The bedform migration vectors (indicated by dune displacement) and thus sediment
796 transport pathways strongly agreed with the modelled RTC. Distally from the PF, sediment
797 transport pathways agreed with predominantly southerly net transport (Reynaud &
798 Dalrymple, 2012). However, proximal to the PF, the energetic tidal currents were found to
799 possess RTC vortices that appeared to recirculate sediment upstream by counter currents,
800 inshore of the main flood flow.

801 RTC vortices influencing sediment transport have been identified by other studies (Kubicki et
802 al., 2017; Cruz & Noernberg, 2020). However, this investigation reveals that RTC vortices
803 may have far field influences on sediment transport pathways by recirculating sediment back
804 towards a BLP, limiting the erosional rate of the seabed. Further sediment transport studies in
805 this area should focus on explaining the minor spatial discrepancies between the inferred
806 sediment transport pathways and the RTC. This may be explainable by considering wave-
807 driven transport and baroclinic flows which was deemed beyond the scope of this study.

Nonetheless, this investigation has highlighted the importance of considering the local sediment transport field as well as the broader transport pathway when performing a site assessment for nearshore and offshore development. Insights offered here may be useful when considering offshore development at this study site and other areas that are proximal to a BLP. The upstream sediment starvation by disruption of the recirculatory sediment transport stream may have pronounced effects on offshore construction. Especially in constrained coastal areas (e.g. estuaries) where local flow modifications may have pronounced effects on particularly starved sediment streams.

7 Acknowledgement

This study presents data available from the UK Hydrographic Office (UKHO) and thus contains public sector information, licensed under the Open Government Licence v3.0, the owners of which are listed in table 1. Depth data was also downloaded from EMODnet Bathymetry Consortium (2020): EMODnet Digital Bathymetry (DTM). Seabed geophysical data was collected from British Geological Society (BGS) and thus contains British Geological Survey materials ©NERC 2021. Timeseries bathymetry data was supplied by Southern and Scottish Electricity Networks (SSEN) which approves the results reported here. British Oceanographic Data Centre (BODC) are the data custodians for the ADCP dataset reported here, publicly available under data license ©BODC 2021. The research here was funded by the Scottish Universities Partnership for Environmental Research (SUPER) DTP in partnership with the University of the Highlands and Islands (UHI) and Scottish Association for Marine Science (SAMS). The authors lastly give thanks to the reviewers for providing invaluable feedback on the research.

8 References

Armstrong, C., Howe, J., Dale, A. & Allen, C. (2021). Bathymetric observations of an extreme tidal flow: approaches to the Gulf of Corryvreckan, western Scotland, UK. Continental Shelf Research. 212. Doi: 10.1016/j.csr.2021.104347

Adcock, T. A. A., Draper, S., Houlsby, G. T., Borthwick, A. G. L. & Serhadlioglu, S. (2013). The available power from tidal stream turbines in the Pentland Firth. Proceedings of the Royal Society A: Mathematical, Physical and Engineering Sciences. 469(2157). Doi: 10.1098/rspa.2013.0072

Allen, J. R. L. (1980). Sand waves: A model of origin and internal structure. Sedimentary Geology. 26(4), pp. 281-328.

Ashley, G. M. (1990). Classification of large-scale subaqueous bedforms; a new look at an old problem. Journal of Sedimentary Research. 60(1), pp. 160-172. Doi: 10.2110/jsr.60.160

Bastos, A., Collins, M. & Kenyon, N. (2003). Water and sediment movement around a coastal headland, Portland Bill, southern UK. Ocean Dynamic. 53, pp. 309-321. Doi: 10.1007/s10236-003-0031-1.

Belderson, R. H. & Stride, A. H. (1966). Tidal current fashioning of a basal bed. Marine Geology. 4(4), pp. 237-257. Doi: 10.1016/0025-3227(66)90044-2

Belderson R. H., Johnson M. A. & Kenyon N. H. (1982), Bedforms, in Stride A.H. ed., Offshore tidal sands : London Chapman & Hall p. 27– 57.

853 Berthot, A. & Pattiaratchi, C. (2006). Field measurements of the three-dimensional
854 current structure in the vicinity of a headland-associated linear sandbank. Continental
855 Shelf Research. 26(3), pp. 295-317. Doi: 10.1016/j.csr.2005.11.010.

856 Boguchwal, L. A. & Southard, J. B. (1990). Bed configurations in steady unidirectional
857 water flows; part 1, scale model study using fine sands. Journal of Sedimentary Research.
858 60 (5), pp. 649-657. Doi: 10.1306/212F923C-2B24-11D7-86480001.02C1865D

859 British Geological Survey (2021). Pentland Firth (Seabed bedrock 1:250k), Available:
860 https://www.bgs.ac.uk/datasets/marine-bedrock-250k/.

861 British Oceanographic Data Centre (2017). Underway Acoustic Doppler Current Profiler
862 (ADCP) data from Pentland Firth, April to October 2009. https://data-
863 search.nerc.ac.uk:443/geonetwork/srv/api/records/59536fdbe1965412bc9f69389c666237

864 Buijsman, M. C. & Ridderinkhof, H. (2008). Long-term evolution of sand waves in the
865 Marsdiep inlet. I: High-resolution observations. Continental Shelf Research. 28(9), pp.
866 1190-1201. Doi: 10.1016/j.csr.2007.10.011.

867 Courant, R., Friedrichs, K. O. & Lewy, H. (1928). Ueber die partiellen
868 Differenzgleichungen der mathematische Physik. Math Ann. 100, pp. 32–74

869 Cheng, P., Gao, S. & Bokuniewicz, H. (2004). Net sediment transport patterns over the
870 Bohai Strait based on grain size trend analysis. Estuarine, Coastal and Shelf Science.
871 60(2), pp. 203-212. Doi: 10.1016/j.ecss.2003.12.009.

872 Coleman, S. E. & Melville, B. W. (1996). Initiation of Bed Forms on a Flat Sand Bed.
873 Journal of Hydraulic Engineering. 122 (6), 301.

874 Couldrey, A. J., Benson, T., Knaapen, M. A. F., Marten, K. V. & Whitehouse, R. J. S.
875 (2020). Morphological evolution of a barchan dune migrating past an offshore wind farm

876 foundation. Earth Surface Processes and Landforms. 45(12), pp. 2884-2896. Doi:
877 10.1002/esp.4937.

878 Cruz, O. G. & Noernberg, A. M. (2020). Bedforms controlled by residual current vortices
879 in a subtropical estuarine tidal channel. Estuarine, Coastal and Shelf Science.
880 232(106485). Doi: 10.1016/j.ecss.2019.106485.

881 Daniell, J. J. (2015). Bedload parting in western Torres Strait, northern Australia.
882 Continental Shelf Research. 90, pp. 58-69. Doi: 10.1016/j.csr.2014.11.008

883 Deltares (2014). Delft3D-FLOW User Manual, Hydro-morphodynamics, Version
884 3.15.34158. Technical document. Accessible:
885 http://content.oss.deltares.nl/delft3d/manuals/Delft3D-FLOW_User_Manual.pdf.

886 Duffy, G. P. & Hughes-Clarke, J. E. (2005). Application of spatial cross correlation to
887 detection of migration of submarine sand dunes. Journal of Geophysical Research.
888 110(F4). Doi: 10.1029/2004JF000192.

889 Easton, M. C., Woolf, D. K. & Bowyer, P. A. (2012). The dynamics of an energetic tidal
890 channel, the Pentland Firth, Scotland. Continental Shelf Research. 48, pp. 50–60. Doi:
891 10.1016/j.csr.2012.08.009.

892 Fairley, I., Masters, I. & Karunarathna, I. (2015). The cumulative impact of tidal stream
893 turbine arrays on sediment transport in the Pentland Firth. Renewable Energy. 80, pp.
894 755-769.

895 Fenster, M. S., Fitzgerald, D. M., Bohlen, D. F., Lewis, R. S. & Baldwin, C. T. (1990).
896 Stability of giant sand waves in eastern Long Island Sound, U.S.A. Marine Geology. 91
897 (3), 207-225.

898 Flemming, B. (2000). The role of grain size, water depth and flow velocity as scaling
899 factors controlling the size of subaqueous dunes. In: Trentesaux, T. Garlan (Eds.), Marine
900 Sandwave Dynamics, University of Lille 1 (France), proceedings (2000), pp. 55-60.

901 Folk, R. L. & Ward, W. C. (1957). Brazos River bar [Texas]; a study in the significance
902 of grain size parameters. Journal of Sedimentary Research. 27(1), pp. 3-26. Doi:
903 10.1306/74D70646-2B21-11D7-8648000102C1865D.

904 Gao, S. & Collins, M. B. (1994). Analysis of grain size trends, for defining sediment
905 transport pathways in marine environments. Journal of Coastal Research. 10(1), pp. 70–
906 78. Doi: 10.2307/4298194

907 Gao, S., Collins, M. B., Lanckneus, J., De Moor, G. & Van Lancker, V. (1994) Grain size
908 trends associated ith net sediment transport patterns: An example from the Belgian
909 continental shelf. Marine Geology. 121(3-4), pp. 171-185.

910 Guillou, N. & Chapalain, G. (2010). Numerical simulation of tide-induced transport of
911 teterogeneous sediments in the English Channel. Continental Shelf Research. 30(7), pp.
912 806-819.

913 Harris, P. T. (1988). Sediments, bedforms and bedload transport on the continental shelf
914 adjacent to Torres Strait, Australia – Papua New Guinea. Continental Shelf Research,
915 8(8), pp. 979-1003. Doi: 10.1016/0278-4343(88)90058-1.

916 Harris, P. T. & Collins, M. B. (1984). Bedform distributions and sediment transport paths
917 in the Bristol Channel and Severn Estuary, UK. Marine Geology. 62(1-2), pp. 153-166.
918 Doi: 10.1016/0025-3227(84)90059-8

Harris, P. T., Pattiaratchi, C., Collins, M. B., Dalrymple, R. W. (1995). What is a bedload parting? In: Flemming, B. W., Bartholoma, A. (eds.), Tidal Signatures in Modern and Ancient Sediments. Blackwell Science, pp. 3–18.

Hino, M. (1968). Equilibrium-range spectra of sand waves formed by flowing water. Journal of Fluid Mechanics. 34 (2), 565-573.

Hong, J. H., Chiew, Y. M., Yeh, P. H. & Chan, H. C. (2017). Evolution of local pier-scour depth with dune migration in subcritical flow conditions. Journal of Hydraulic Engineering. 143(4). Doi: 10.1061/(ASCE)HY.1943-7900.0001261.

Hooke, J. M., Bray, M. J. & Carter, D. J. (1996). Sediment transport analysis as a component of coastal management – a UK example. Environmental Geology. 27, pp. 347-357. Doi: 10.1007/BF00766704

Huijts, K. M. H., Schuttelaars, H. M., de Swart, H. E. & Friedrichs, C. T. (2009). Analytical study of the transverse distribution of along-channel and transverse residual flows in tidal estuaries. Continental Shelf Research. 29(1), pp. 89-100. Doi: 10.1016/j.csr.2007.09.007

Jones, J. E. & Davies, A. M. (2008). On the modification of tides in shallow water regions by wind effects. Journal of Geophysical Research. 113(C5). Doi: 10.1029/2007JC0043104

Kennedy, J. F. (1963). The mechanics of dunes and antidunes in erodible-bed channels. Journal of Fluid Mechanics. 16 (4), pp. 521-544.

King, E., Conley, D., Masselink, G., Leonardi, N., McCarroll, R. J. & Scott, T. (2019). The impact of waves and tides on residual sand transport on a sediment-poor, energetic

941 and macrotidal continental shelf. Journal Geophysical Research Ocean. 124, pp. 4974-
942 5002. Doi: 10.1029/2018JC014861

943 Kubicki, A., Kosters, F. & Bartholoma, A. (2017). Dune convergence/divergence
944 controlled by residual current vortices in the Jade tidal channel, south-eastern North Sea.
945 Geo-Marine Letters. 37, pp. 47-58. Doi: 10.1007/s00367-016-0470-6.

946 Kumbhakar, M., Ghoshal, V. P. & Singh, V. P. (2017). Renyi entropy and random walk
947 hypothesis to study suspended sediment concentration. Journal of Hydrologic
948 Engineering. 22(8). Doi: 10.1061/(ASCE)HE.1943-5584.0001546.

949 Leckie, S. H. F., Mohr, H., Draper, S., McLean, D. L., White, D. J. & Cheng, L. (2016).
950 Sedimentation-induced burial of subsea pipelines: Observations from field data and
951 laboratory experiments. Coastal Engineering. 114, pp. 137-158. Doi:
952 10.1016/j.coastaleng.2016.04.017

953 Le Roux, J. P. & Rojas, E. M. (2007). Sediment transport patterns determined from grain
954 size parameters: overview and state of the art. Sedimentary Geology. 202(3), pp. 473-488.
955 Doi: 10.1016/j.sedgeo.2007.03.014.

956 Leonardi, N., Kolker, A. S. & Fagherazzi, S. (2015). Interplay between river discharge
957 and tides in a delta distributary. Advances in Water Resources. 80, pp. 69-78. Doi:
958 10.1016/j.advwatres.2015.03.005

959 Li, M. Z., Shaw, J., Todd, B. J., Kostylev, V. E. & Wu, Y. (2014). Sediment transport and
960 development of banner banks and sand waves in an extreme tidal system: Upper Bay of
961 Fundy, Canada. Continental Shelf Research. 83, pp. 86-107. Doi:
962 10.1016/j.csr.2013.08.007.

963 Mirzania, P., Ford, A., Andrews, D., Ofori, G. & Maidment, G. (2019). The impact of
964 policy changes: The opportunities of Community Renewable Energy projects in the UK
965 and the barriers they face. Energy Policy, 129, pp. 1282-1296.
966 Doi:10.1016/j.enpol.2019.02.066

967 Perkol-Finkel, S., Hadary, T., Rella, A., Shirazi, R. & Sella, I. (2018). Seascape
968 architecture – incorporating ecological considerations in design of coastal and marine
969 infrastructure. Ecological Engineering, 120, pp. 645-654. Doi:
970 10.1016/j.ecoleng.2017.06.051

971 Pingree, R. D. (1978). The formation of the shambles and other banks by tidal stirring of
972 the seas. Journal of Marine Biology Association. 58, pp. 211-226.

973 Pingree, R. D. & Griffiths, D. K. (1979). Sand transport paths around the British Isles
974 resulting from M2 and M4 tidal interactions. Journal of the Marine Biological
975 Association of the United Kingdom, 59(2), 497–. Doi: 10.1017/s0025315400042806

976 Pye, S., Li, F. G. N., Price, J. & Fais, B. (2017). Achieving net-zero emissions through
977 the reframing of UK national targets in the post-Paris Agreement era. Nature Energy,
978 2(3), pp 117024. Doi:10.1038/nenergy.2017.24

979 Reynaud, J. Y. & Dalrymple, R. W. (2012). Shallow-Marine Tidal Deposits. In: Davis Jr.
980 R. & Dalrymple, R. (eds), Principles of Tidal Sedimentology. Springer, Dordrecht. Doi:
981 10.1007/978-94-007-0123-6_13

982 Sakhaee, F. & Khalili, F. (2021). Sediment pattern and rate of bathymetric changes due to
983 construction of a breakwater extension at Nowshahr port. Journal of Ocean Engineering
984 and Science, 6(1), pp. 70-84.

985 Schmitt, T. & Mitchell, N. C. (2014). Dune-associated sand fluxes at the nearshore
986 termination of a banner sand bank (Helwick Sands, Bristol Channel). Continental Shelf
987 Research. 76, pp. 64-74. Doi: 10.1016/j.csr.2014.01.003.

988 Shaw, J., Todd, B. J., Li, M. Z. & Wu, Y. (2012). Anatomy of the tidal scour system at
989 Minas Passage, Bay of Fundy, Canada. Marine Geology. 323-325, pp. 123-134. Doi:
990 10.1016/j.margeo.2012.07.007

991 Signell, R. & Geyer, R. W. (1991). Transient eddy formation around headlands. Journal
992 of Geophysical Research. 96(C2), pp. 2561-2575. Doi:10.1029/90JC02029.

993 Thiébot, J., Bailly du Bois, P. & Guillou, S. (2015). Numerical modelling of the effect of
994 tidal stream turbines on the hydrodynamics and the sediment transport- application to the
995 Alderney Race (Raz Blanchard), France. Renewable Energy. 75, pp. 356-365. Doi:
996 10.1016/j/renene.2014.10.021

997 Traoré, K., Menier, D., Gensac, E., Le Roy, P., Lambert, C., Bessin, P., Pedoja, K.,
998 Duperret, A. & Le Gall, R. (2021). Evolution of a Holocene banner bank controlled by
999 morphodynamics and structural setting of a macrotidal coast: Saint-Brieuc Bay (NW-
1000 Europe). Geoscience Frontiers. 12(5). Doi: 10.1016/j.gsf.2021.101183

1001 Van den Berg, J. H. (1987). Bedform migration and bedload transport in some rivers and
1002 tidal environments. Sedimentology. 34, pp. 681-698.

1003 Van Dijk, T. A. G. P. & Lindenbergh, R. C. (2017). Methods for analysing bedform
1004 geometry and dynamics. In: Guillén, J., Acosta, J., Chiocci, F., & Palanques, A., (eds),
1005 Atlas of Bedforms in the Western Mediterranean. Springer, Cham. Doi: 10.1007/978-3-
1006 319-33940-5_2

Van Landeghem, K. J. J., Uehara, K., Wheeler, A. J., Mitchell, N. C., & Scourse, J. D. (2009). Post-glacial sediment dynamics in the Irish Sea and sediment wave morphology: Data–model comparisons. Continental Shelf Research. 29(14), pp. 1723–1736. Doi: 10.1080/17445647.2020.1758811

Van Landeghem, K. J. J., Baas, J. H., Mitchell, N. C., Wilcockson, D. & Wheeler, A. J. (2012). Reversed sediment wave migration in the Irish Sea, NW Europe: a reappraisal of the validity of geometry-based predictive modelling and assumptions. Marine Geology. 295-298(1), pp. 95-112

Vittori, G. & Blondeaux, P. (1990). Sand ripples under sea waves Part 2. Finite-amplitude development. Journal of Fluid Mechanics. 218, pp. 19-39.

Wang, W., Yang, J., Zhao, M., Dong, L., Min, J. & Huang, E. (2020). Spatial variation in grain-size population of surface sediment from northern Bering Sea and western Arctic Ocean: implications for provenance and depositional mechanisms. Marine Earth Science. 31(3), pp. 192-204. Doi: 10.13679/j.advps.2020.0015.

Yalin, M. S. (1964). Geometrical Properties of Sand Wave. Journal of the Hydraulics Division. 90 (5), 105-119.

1029 Figure Captions

1030 [1]. Bathymetry data from UKHO superimposed atop EMODnet bathymetry, covering study
1031 area of the eastern approach to the Pentland Firth and Orkney. Pentland Firth's location
1032 within the UK is depicted in the inset figure. The black solid boxes index to subsequent
1033 figures whereas the dashed box indicates area of timeseries bathymetric data.

1034 [2]. Digitised bedforms of the study area identified to be the likely product of the strong tidal
1035 streams. Notice the *very large dunes* furthest east in the study domain: these are situated at
1036 the edge of a significant deepening of the bathymetry and may be the product bathymetrically
1037 intensified tidal currents accelerated by the shallowing seabed and/or wave-induced sediment
1038 transport. **Medium dunes* are the smallest bedform identified in the dataset with
1039 identification limited to areas covered by the timeseries (highest resolution) bathymetry. It is
1040 suspected these bedforms exist elsewhere in the study domain but were missed due to low
1041 resolution data.

1042 [3]. Sediment type of eastern approach to Pentland Firth. (Top) Coloured circles indicate
1043 location and classification of sediment samples atop a greyscale bathymetry for reference.
1044 The dashed black square indicates the location of the interpolated domain (bottom).

1045 [4]. Bathymetry data of identified bedforms found within the study site. [4A] Noss Head dune
1046 field with dashed rectangles indicating subsequent subfigures. [4B] higher resolution field of
1047 view of area as indicated in [4A]. [4C] Higher resolution field of view of area as indicated in
1048 [4A]. [4D] Arcuate Bank located east of Pentland Firth (also shown in fig. 5). [4E] Dune field
1049 located east of Orkney (also shown in fig. 7).

1050 [5]. Arcuate Bank bathymetry [5A] with the grey dashed box outlining the FOV for 5B, slope
1051 [5B] and depth profiles [5C]. Depth profiles are indexed in figure [5A]. Note that the depth

profiles are not aligned due to the prohibitively varying scales of bedforms. The deep depressions are located west of the depth profile 7-8.

[6]. Bathymetry [6A], depth profile [6B], elevation difference [6C] and digitised slope [6D] of bedforms found north of Noss Head. Depth profiles and figures [6C] and [6D] are indexed within [6A].

[7]. Bathymetry [7A], depth profile [7B], elevation difference [7C] and digitised slope [7D] of medium dunes found east of Orkney (indicated in figure 2).

[8]. Results of spatial cross correlation. The annotated map shows the transect of timeseries bathymetry extending east from northeast Scotland before turning north to track parallel to Orkney's east coast. Vectors are coloured by migration rate (m/yr) and projected on to the bathymetric slope. Red squares show indexed subfigures. [8A] Noss Head dune field showing north west displacement to the northwest of the sample area, and southward displacement to the south. [8B] Southeast of the Pentland Firth with displacement oriented south easterly. [8C] East southeast of Pentland Firth with displacement weakly oriented west with a change in direction to the south of the sample area to the southeast. [8D] East of Orkney, with consistently southward displacement.

[9]. Flow model validation with ADCP data. [9A] Location of three ADCP transects used for model validation with the circles indicating data point locations and stars indicating the start of the transect (see figure [9D]). [9B] Location of ADCP sampling site relative to Stroma Island superimposed onto model output of the ebb tide with the red dashed box indexing [9C]. [9C] ADCP – 2 transect superimposed on model – 2 output with both circle and contour colours relating to flow speed (m/s) from ADCP and model, respectively. [9D] Comparison of simulated flow speeds with ADCP transects 1, 2 and 3.

[10]. Flow model results. For all panels, white areas indicate landmass. [10A] Depth of model domain. [10B] Residual tidal flow field with colours relating to flow speed (m/s) and black arrows indicating direction. [10C] As [10B] for flood tidal flow field. [10D] As [10B] for ebb tidal flow field.

[11]. Residual tidal current (RTC) flow field superimposed atop EMODnet bathymetry. Also indicated are the sediment transport pathways inferred from bedform migration analysis, and the position of the two identified banner banks, extending into the eastern approach of the Pentland Firth.

Figure 1 - study map

Click here to access/download;Figure;1.png

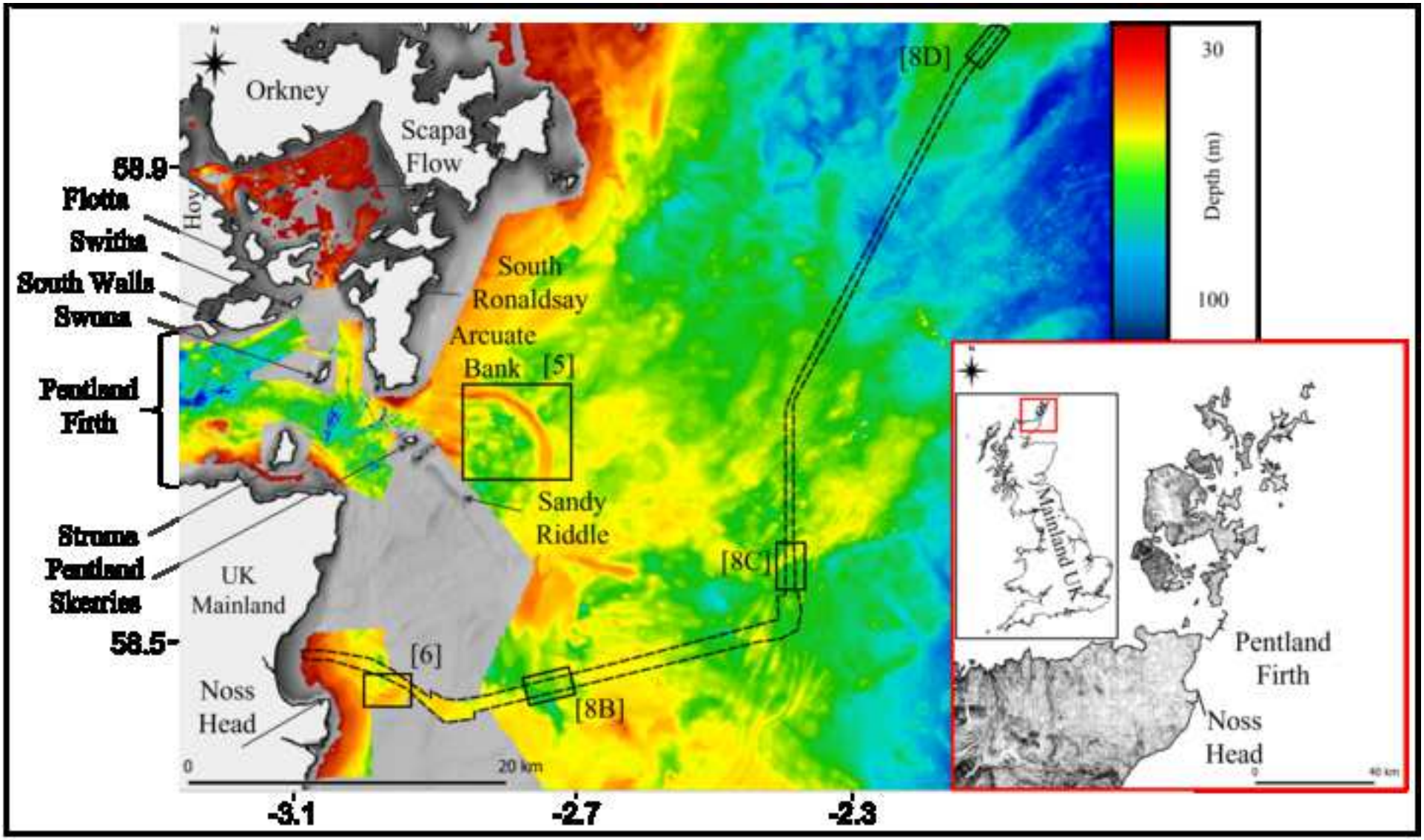

Figure 2 - bedform distribution

Click here to access/download;Figure;2.png

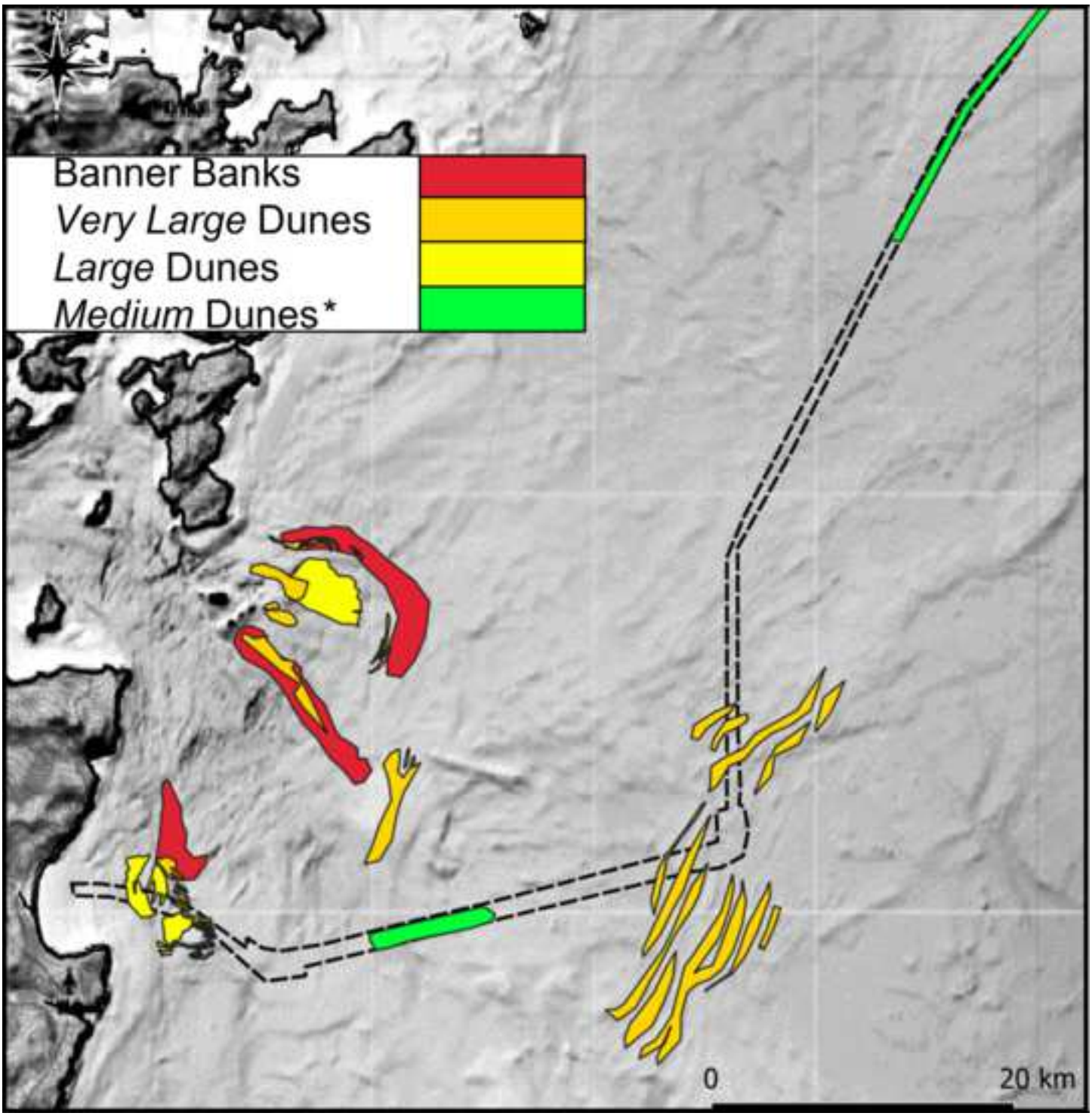

Figure 3 - sediment type

Click here to access/download;Figure;3.png

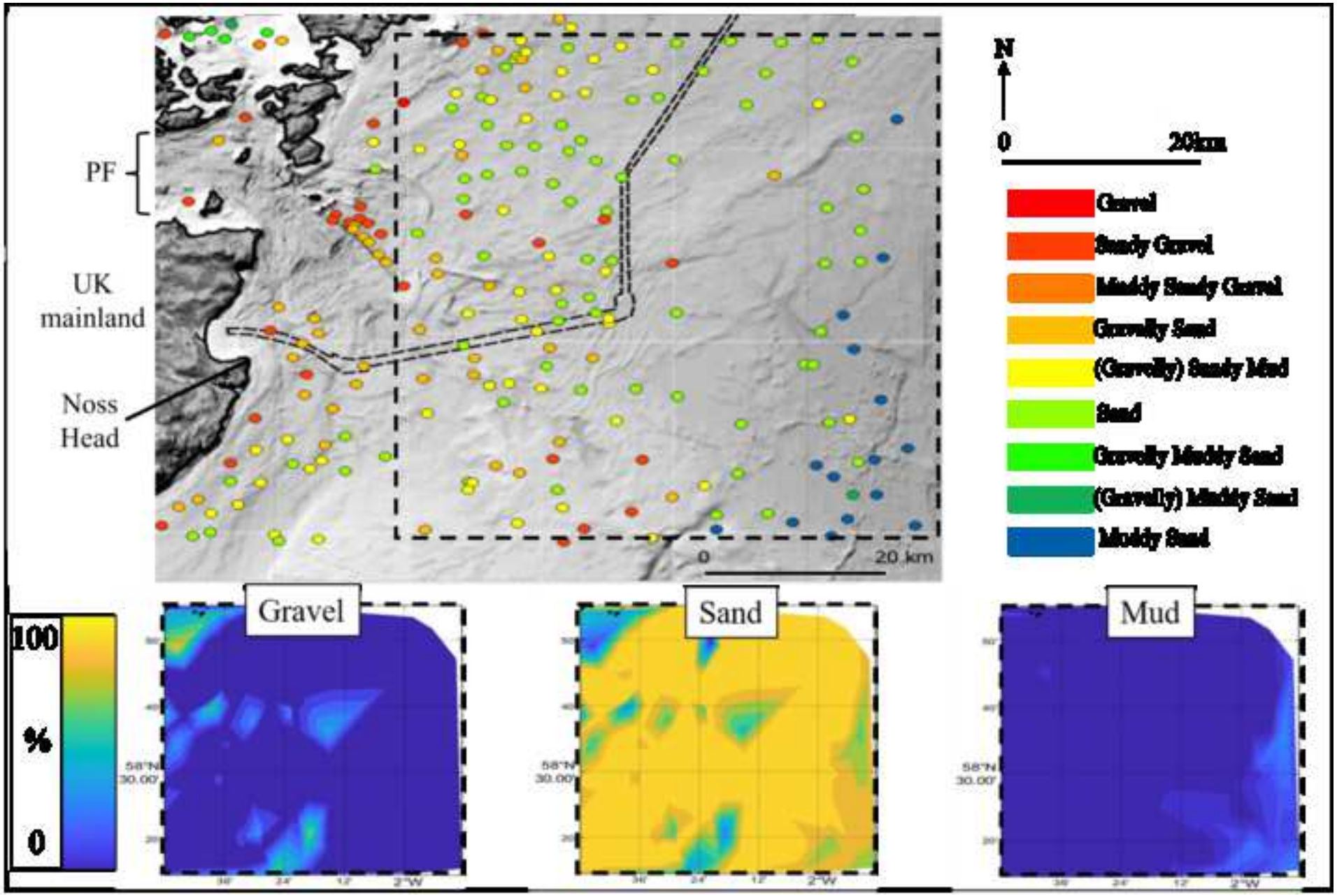

Figure 4 - bedforms

Click here to access/download;Figure;4.png

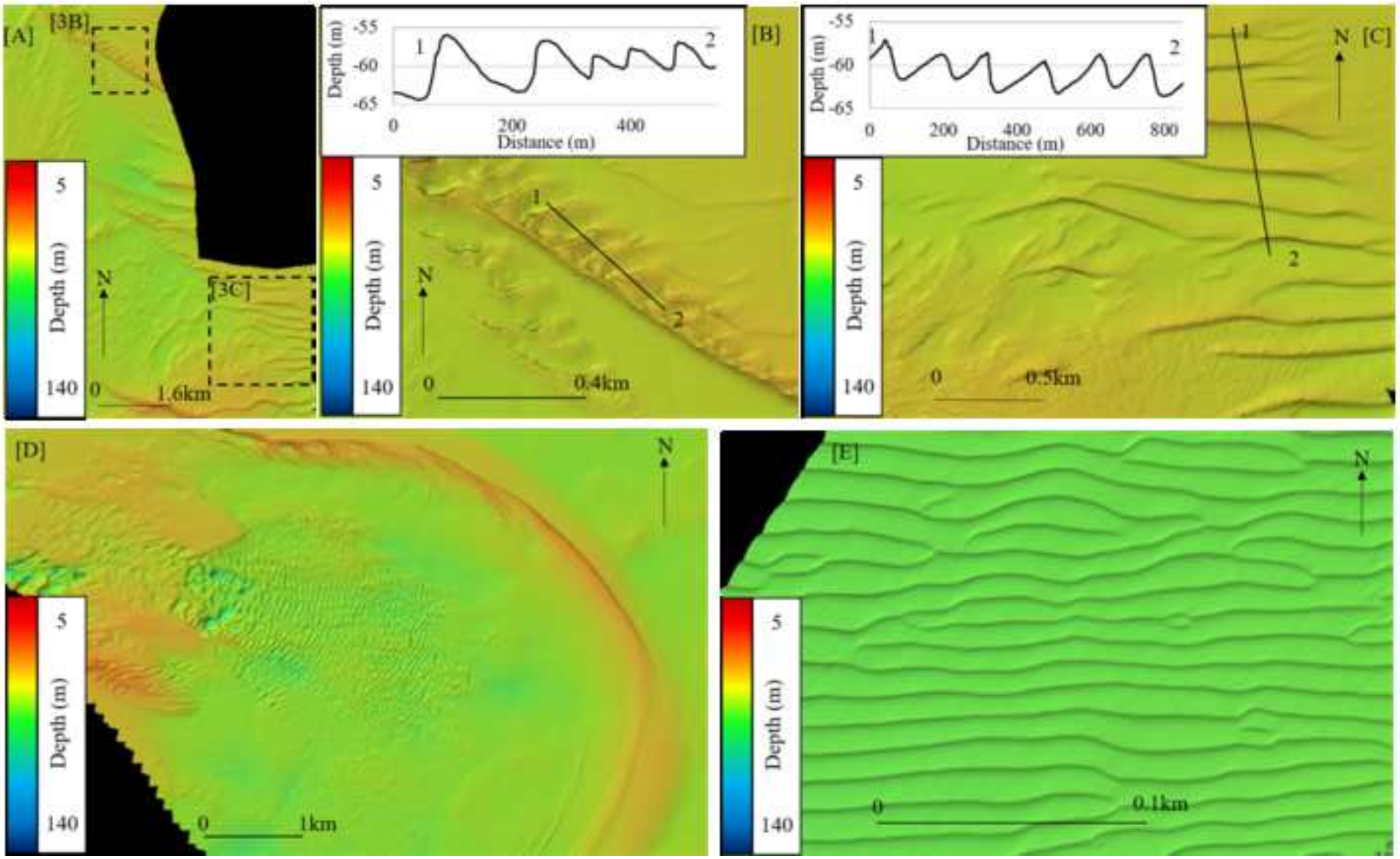

Figure 5 - arcuate bank

Click here to access/download;Figure;5.png

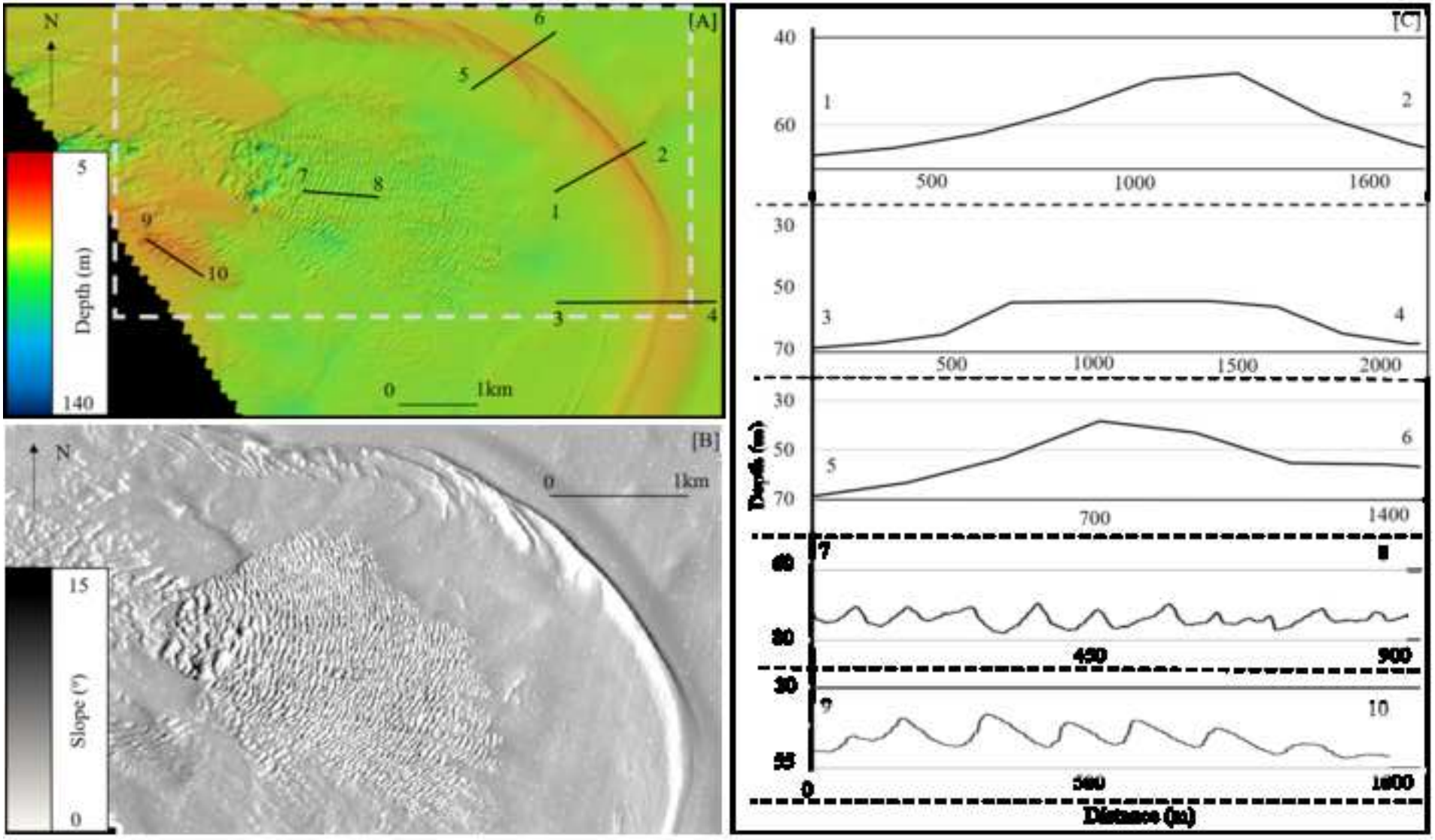

Figure 6 - Noss Head dunes

Click here to access/download;Figure;6.png

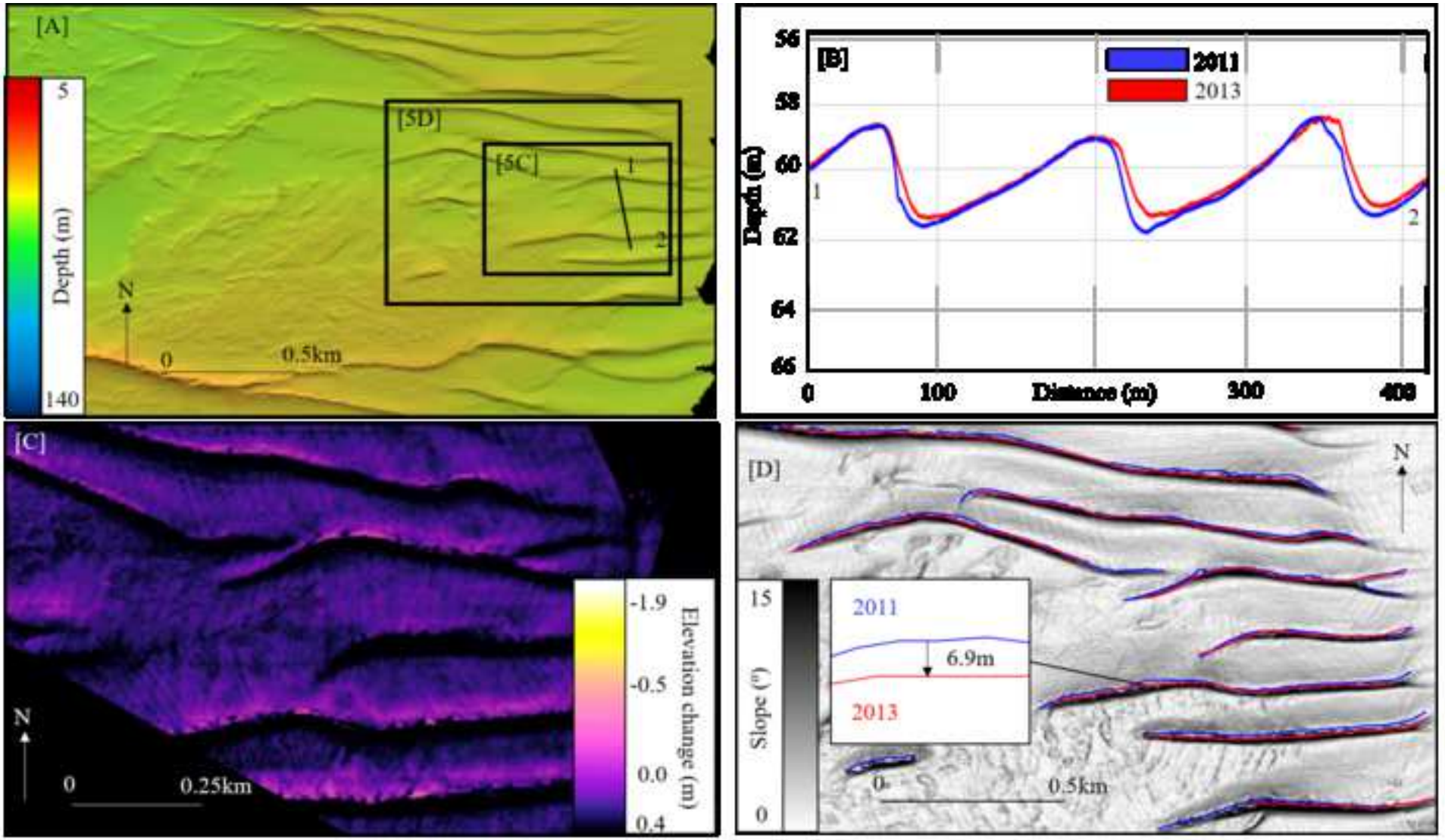

Figure 7 - E.Orkney dunes

Click here to access/download;Figure;7.png

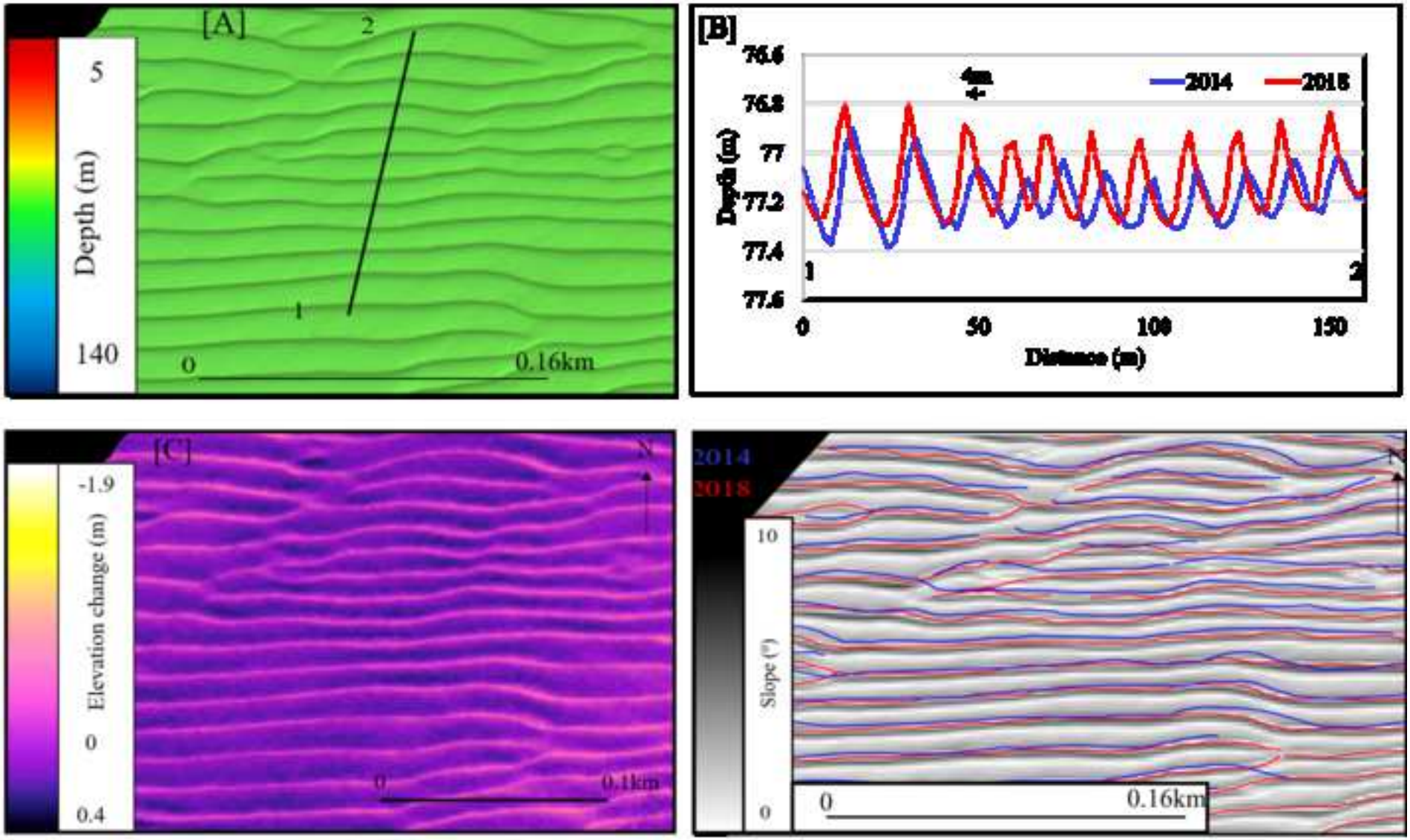

Figure 8 - XCorr Outputs

Click here to access/download;Figure;8.png

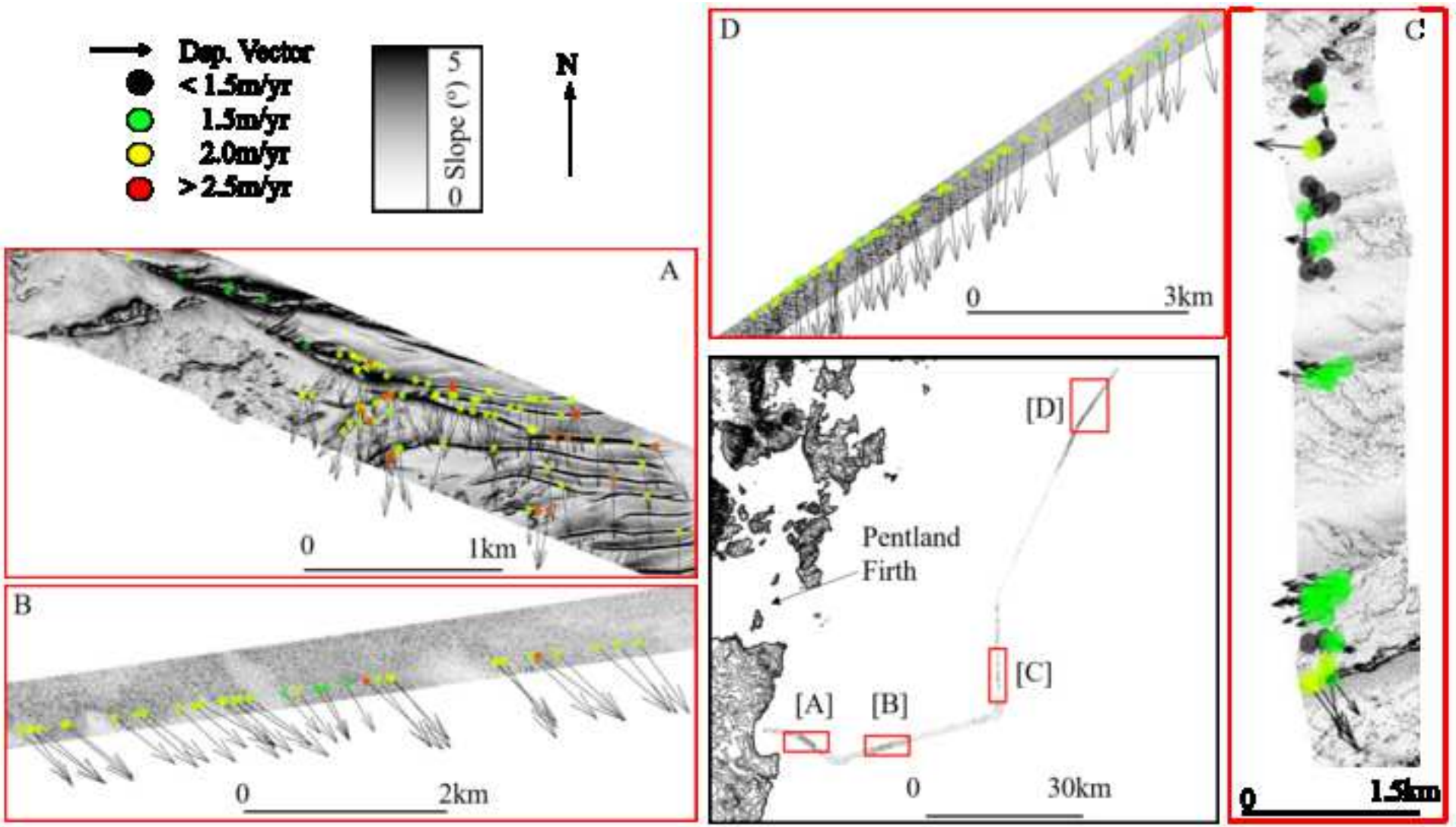

Figure 10 - Model outputs

Click here to access/download;Figure;10.png

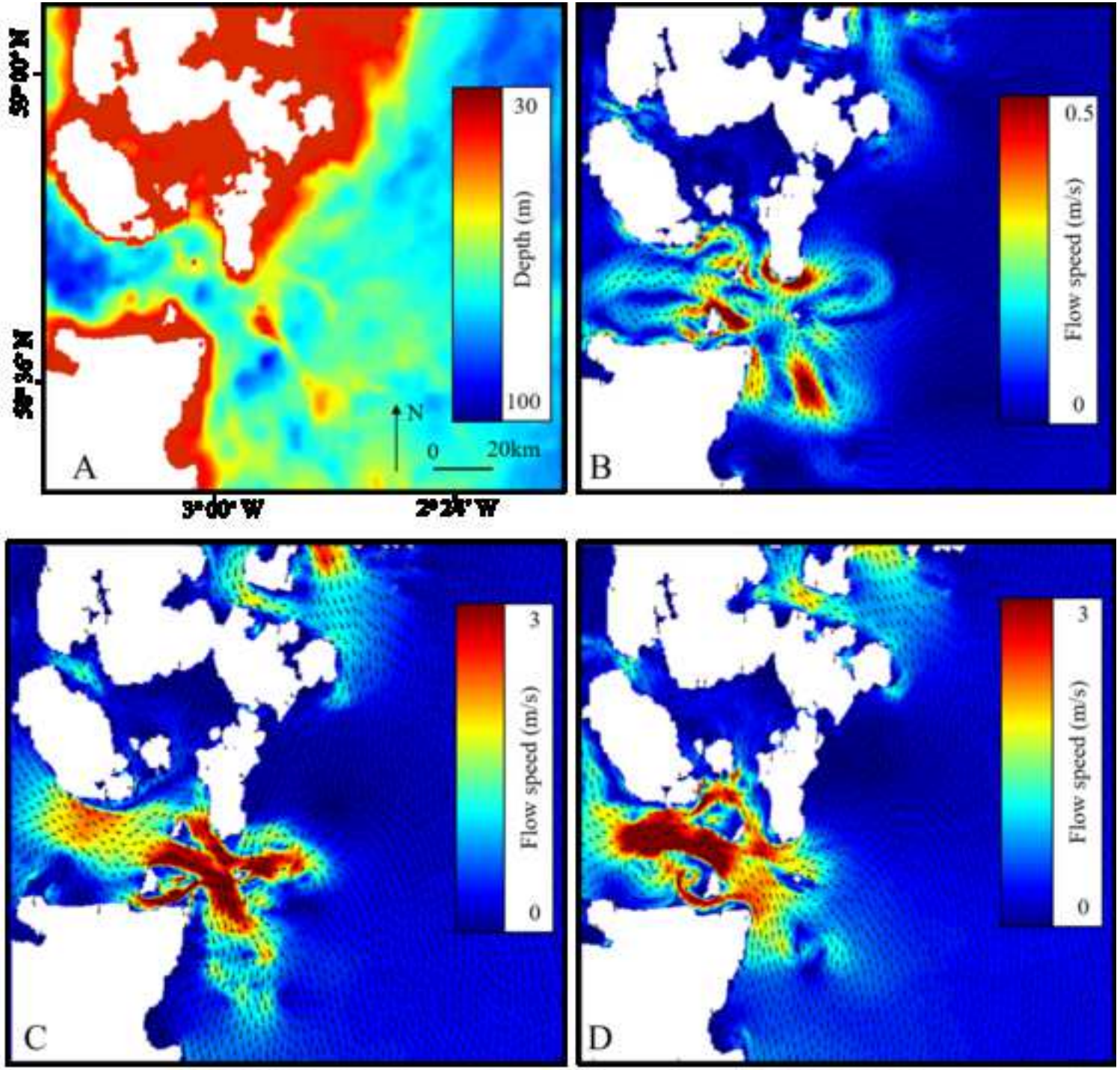

Figure 11 - Model + Bathy

Click here to access/download;Figure;11.png

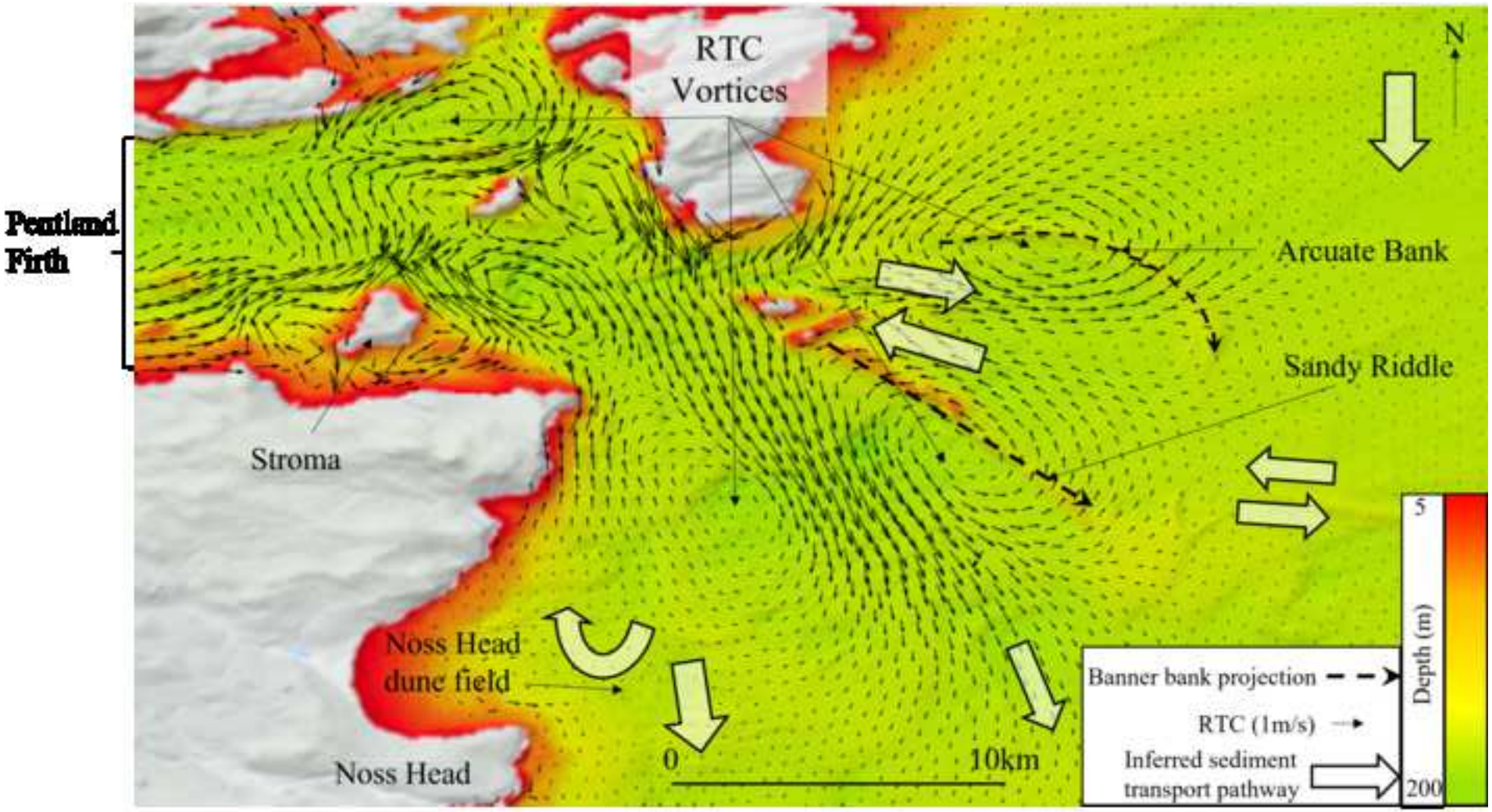

Figure 9 - Model validation

Click here to access/download;Figure;9.png

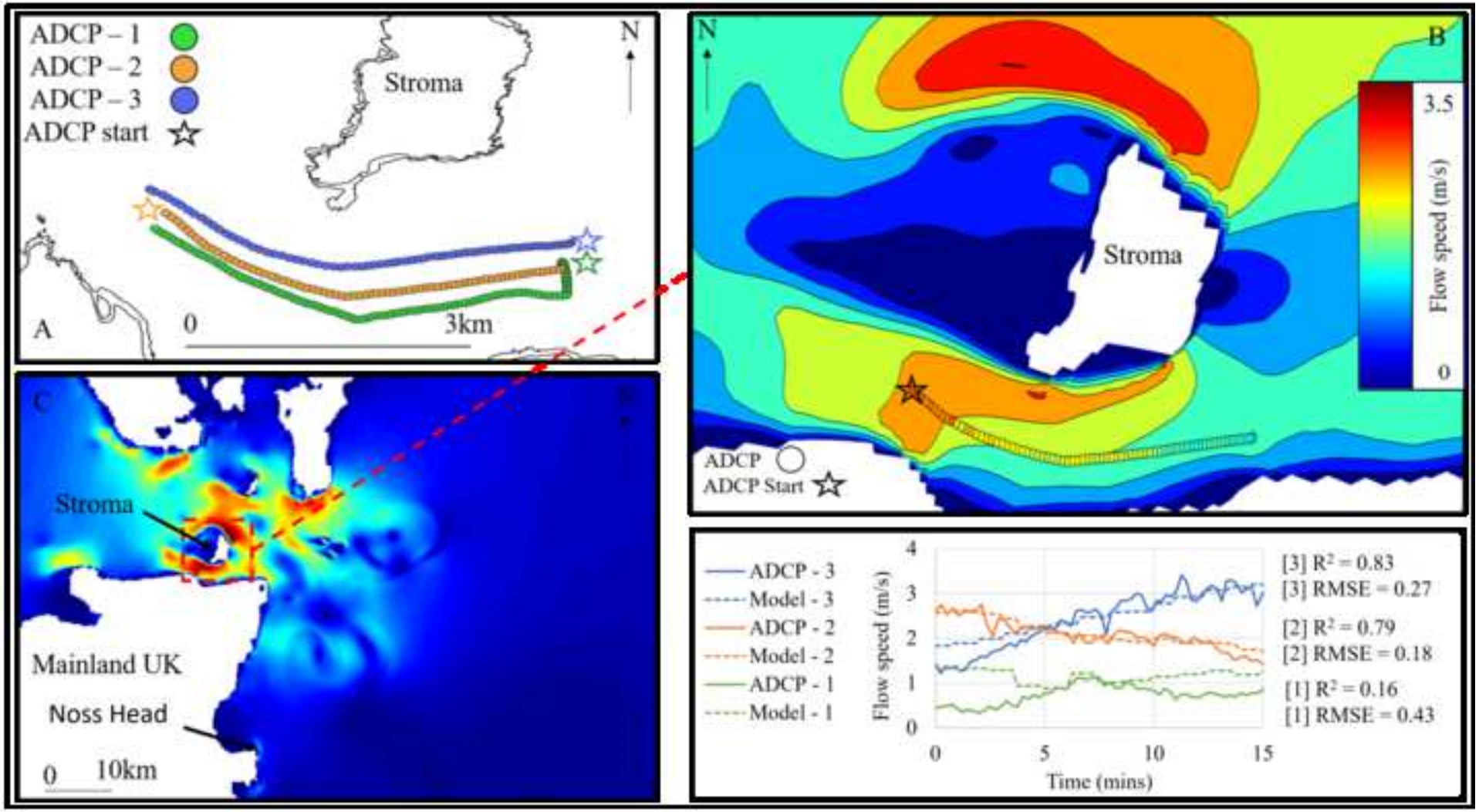

Table 1). Bathymetric datasets from UKHO with ID, geographical extents (where A and B are minimum and maximum values, respectively), collecting organisation, spatial resolution, and date collected.

Bathymetry data ID	**Geographical extent (WGS 1984 in decimal degrees [dd.dddd]) [lonA : lonB, latA : latB]**	**Data collection**	**Spatial resolution (m)**	**Date collected [dd mm yyyy]**
2006 HI1137 Eastern Approaches to Sanday and Stronsay Blk1	[-2.5464 : -1.8267, 58.9767 : 59.3532]	Netsurvey	2	08 08 2005 – 30 07 2006
2006 HI1137 Eastern Approaches to Sanday and Stronsay Blk2	[-2.3755 : -1.8406, 58.9820 : 59.2687]	Netsurvey	2	08 08 2005 – 30 07 2006
2006 HI1137 Eastern Approaches to Sanday and Stronsay Blk3	[-1.8455 : -1.4134, 58.9984 : 59.2932]	Netsurvey	2	16 06 2006 – 19 09 2006
2006 HI1137 Eastern	[-2.8394 : -2.0905, 58.7960 : 59.0737	Netsurvey	2	24 06 2006 – 31 08 2006

Approaches to Sanday and Stronsay Blk5				
2006 HI1150 Tarbat Ness to Sarclet Head 2m SB	[-3.8322 : -2.7459, 57.8204 : 58.3544]	Gardline Surveys	2	31 05 2006 – 22 08 2006
2006 HI1150 Tarbat Ness to Sarclet Head 4m SB	[-3.7641 : -2.2808, 57.8200 : 58.3936	Gardline Surveys	4	31 05 2006 – 22 08 2006
2007 HI1202 Westray Firth to Stronsay Firth 2m SB	[-3.0298 : - 2.5592, 58.9093 : 59.2337]	Marin Matteknik	2	09 12 2006 – 05 02 2007
2007 HI1218 Approaches to the Orkney Islands Blk1	[-2.9357 : -2.0956, 58.5812 : 58.8005]	Netsurvey	2	28 04 2007 – 02 06 2007
2008 HI1137 Eastern Approaches to Sanday and Stronsay Blk4	[-2.1045 : -1.4261, 58.7967 : 59.0019]	Netsurvey	2	31 07 2008 – 22 08 2008

2008 HI1137 Eastern Approaches to Sanday and Stronsay Blk6	[-2.8374 : -1.8414, 58.5811 : 58.8039	Netsurvey	2	22 08 2008 – 08 09 2009
2009 2010-027833 Kirkwall Bay Orkneys	[-3.0616 : -2.8019, 58.9621 : 59.0470]	Fathoms	2	04 06 2009 – 12 08 2009
2009 2010-027833 Scapa Flow Area2A 2m SB	[-3.2683 : -2.8954, 58.8118 : 58.9586	Fathoms	2	04 06 2009 – 12 08 2009
2009 2010-027833 Scapa Flow Main Burra 2m SB	[-3.3561 : -3.2026, 58.8994 : 58.9707]	Fathoms	2	04 06 2009 – 12 08 2009
2009 2011-147366 Isle of Stroma Pentland Firth	[-3.337 : -2.8904, 58.6389 : 58.7907]	Marine Scotland	2	18 07 2009 – 05 08 2009
2011 2017-310912 Noss Head 2m	[-3.0945 : -2.9251, 58.4129 : 58.5365	British Geological Society	2	09 08 2011 – 17 08 2011

2012 HI1372 Moray Firth Block1 2m SB	[-2.8406 : -2.3320, 57.9975 : 58.2276]	Netsurvey	4	07 02 2012 – 04 07 2012
2012 HI1372 Moray Firth Block2 2m SB	[-2.3324 : -1.8912, 57.9991 : 58.2279]	Netsurvey	4	07 02 2012 – 04 07 2012
2012 HI1372 Moray Firth Block3 2m SB	[-1.9087 : -1.2187, 58.0003 : 58.2213]	Netsurvey	4	07 02 2012 – 04 07 2012
2012 HI1372 Moray Firth Blk4 2m SB	[-2.5119 : -1.8132, 58.2219 : 58.3939	Netsurvey	4	07 02 2012 – 04 07 2012
2012 HI1372 Moray Firth Blk5 2m SB	[-2.3322 : -1.8070, 58.3969 : 58.5932	Netsurvey	4	07 02 2012 – 04 07 2012
2012 HI1372 Moray Firth Blk6 2m SB	[-2.8156 : -2.3259, 58.3429 : 58.5920]	Netsurvey	4	07 02 2012 – 04 07 2012

Table 2). First order dune classification system adopted from Ashley (1990).

Dune class	**Wavelength (m)**	**Wave height (m)**

Small	0.6-5.0	0.075-0.400
Medium	5-10	0.40-0.75
Large	10-100	0.75-5.00
Very large	>100	>5

Conflict of Interest

The authors in this paper declare no conflicts of interests.